ORGANOMETALLICS

pubs.acs.org/Organometallics

Article

Hydrogen Bond Patterning and Biological Activity of Ferrocene Conjugates with Homo- and Heterochiral Ala−Pro Dipeptides

Monika Kovačević, Mojca Čakić Semenčić, Martina Bagović, Kristina Radošević, Karla Hanousek Čiča, Jasna Mrvčić, Krešimir Molčanov, Sunčica Roca, Ivan Kodrin,* and Lidija Barišić*

Cite This: *Organometallics* 2024, 43, 2608−2625

Read Online

ACCESS | Metrics & More | Article Recommendations | Supporting Information

ABSTRACT: The chirality of the protein backbone influences both self-assembly and biological activity. In ferrocene-containing peptides, the sequence and chirality of the constitutive amino acids as well as the structure of the ferrocene scaffold strongly influence the conformational properties, whereas the biological activity is more strongly influenced by lipophilicity. A joint spectroscopic and computational study has shown that a relatively simple structural modification, such as changing the order of two amino acids in the dipeptide sequence from Pro−Ala (**III**) to Ala−Pro (**IV**), also alters the hydrogen bonding patterns from a mostly ten-membered (β-turn) to a seven-membered ring (γ-turn), which affects the antiproliferative activity of the ferrocene peptidomimetics studied. A systematic approach presented in this study allowed us to highlight the relevant structural variations that could lead to increased biological activity in similar ferrocene-based bioconjugates.

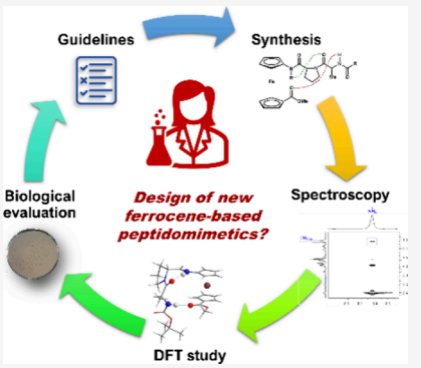

INTRODUCTION

Because of their involvement in most vital cellular processes, protein−protein interactions (PPIs) are widely recognized as the "Holy Grail" of modern life sciences and medicine.[1,2] PPIs take place at an interface hotspot consisting of four to eight amino acids, mainly arranged as turns.[3,4] An error in PPIs can lead to a pathological outcome. Therefore, the identification of hot spot mimetics capable of inhibiting dysfunctional PPIs opens the door to new therapeutic avenues.[4−6]

Turns, the most common structural features in a globular protein, result from the hydrogen bonding (HB) between the carbonyl and amide groups of the polypeptide chain and the reversal of its direction by almost 180°. Being located on the protein surface, the turns are exposed to cell receptors and involved in biological interactions.[7] Several synthetic approaches to the design of the turns have been developed,[8] and one of them is based on the insertion of turn-inducing elements into the peptide chain to facilitate the proper folding and the adoption of the ordered, hydrogen-bonded structure. We have shown that 1,1′-disubstituted ferrocene templates −NH−Fn−CO− and −NH−Fn−NH− (Fn = ferrocenylene) are very potent nucleators of turns and β-sheet-like structures when coupled with amino acids and short peptides.[9−16] Due to the distance between cyclopentadienyl rings of 3.3 Å, the attached hydrogen-bond-accepting and -donating groups come close enough to form inter- and intrastrand hydrogen-bonded (HB) rings of different size in symmetrically disubstituted ferrocene-dipeptide conjugates: a 13-membered HB ring (α-turn), 10-membered HB ring (β-turn), and 7-membered HB ring (γ-turn).[17] We have also found that asymmetrically disubstituted ferrocene peptides participate in various types of hydrogen-bonded turns. Conformational analysis based on experimental (IR, NMR, and CD) and DFT data revealed different conformational patterns for conjugates of methyl 1′-aminoferrocene-carboxylate with Ala (**I**)[18] and Pro (**II**)[19] (Figure 1). While an intrastrand seven-membered HB ring (γ-turn, pattern **A**) was found in both dipeptides **I** and **II**, an additional nine-membered interstrand HB ring (pattern **B**) was observed in the Ala-dipeptide **I**. The moderate influence of the bulkiness and basicity of the Ac and Boc groups was also observed.

The chirality of the backbone controls the self-assembly of proteins so that the substitution of L- with a D-enantiomer or even a minor part of the amino acid sequence can destabilize the self-assembled peptides.[20,21] Cell membranes are composed of chiral, enantiopure biomolecules, so the altering of the peptide backbone chirality could have a strong impact on the biological features. Since the peptide sequence, backbone chirality, and hydrogen-bond-acceptor potential of the N-terminal groups have been found to regulate the size of the HB ring and thus the type of turn in monosubstituted ferrocene conjugates with short peptides,[22,23] we have extended the Ala-peptide **I** with Ac/Boc−L−Pro and Ac/Boc−D−Pro as an

Special Issue: Applied Organometallic Chemistry

Received: June 10, 2024
Revised: July 16, 2024
Accepted: July 18, 2024
Published: August 1, 2024

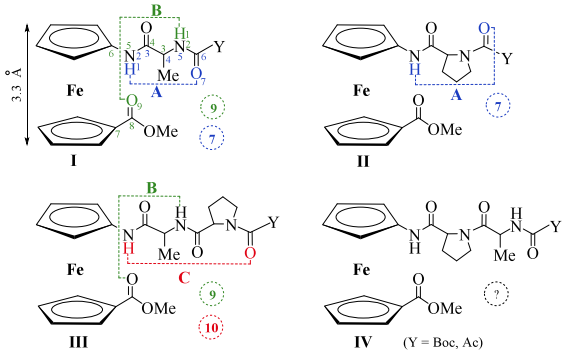

Figure 1. Hydrogen-bonding patterns in asymmetrically disubstituted ferrocene conjugates with Ala (**I**),[18] Pro (**II**),[19] and Pro−Ala dipeptides (**III**).[15] The structure of a new type of asymmetrically disubstituted ferrocene peptides (**IV**) containing homo- and heterochiral Ala−Pro dipeptides.

additional HB acceptor. Both the experimental and computational studies of the resulting peptides **III**[15] showed that (i) the combined HB patterns consisting of intrastrand ten-membered (β-turn, pattern **C**) and interstrand nine-membered rings (pattern **B**) are inherent to the heterochiral Pro−Ala sequence and (ii) the homochiral Pro−Ala sequence resulted in more flexible conformations in which mostly HB pattern **B** occurs (Figure 1).

With this in mind and considering the role of Pro in a tight turn[24] and the Pro−Xaa sequence in a β-turn,[25−27] we have prepared peptides **4**−**11** containing homo- and heterochiral Ala−Pro sequences [type **IV** (Figure 1, Scheme 1)]. Since the

Scheme 1. Synthesis of Homo- (4, 7, 8 and 11) and Heterochiral (5, 6, 9, and 10) Conjugates of Ferrocene-1,1′-diamine with the Ala−Pro Sequence

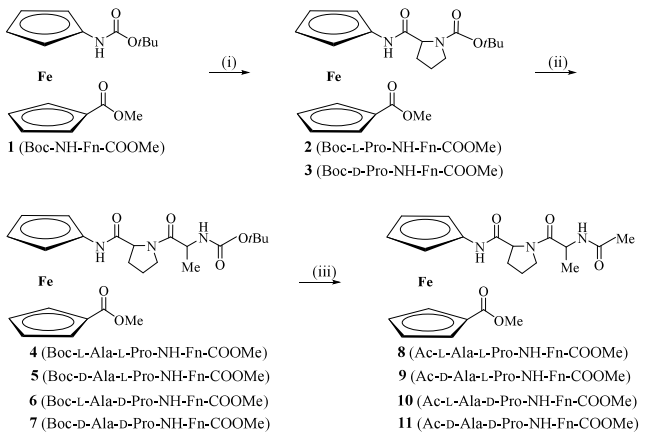

1 (Boc-NH-Fn-COOMe)
2 (Boc-L-Pro-NH-Fn-COOMe)
3 (Boc-D-Pro-NH-Fn-COOMe)
4 (Boc-L-Ala-L-Pro-NH-Fn-COOMe)
5 (Boc-D-Ala-L-Pro-NH-Fn-COOMe)
6 (Boc-L-Ala-D-Pro-NH-Fn-COOMe)
7 (Boc-D-Ala-D-Pro-NH-Fn-COOMe)
8 (Ac-L-Ala-L-Pro-NH-Fn-COOMe)
9 (Ac-D-Ala-L-Pro-NH-Fn-COOMe)
10 (Ac-L-Ala-D-Pro-NH-Fn-COOMe)
11 (Ac-D-Ala-D-Pro-NH-Fn-COOMe)

(i) 1. HCl_{gas}, 2. Et_3N, 3. Boc-(L or D)-Pro-OH, EDC/HOBt;
(ii) 1. HCl_{gas}, 2. Et_3N, 3. Boc-(L or D)-Ala-OH, EDC/HOBt; (iii) 1. HCl_{gas}, 2. NEt_3, 3. AcCl

peptides studied can be considered to be both higher homologues of peptides **II**[19] and constitutionally exchanged peptides **III**,[15] their conformational and biological properties were evaluated, and the obtained results have been compared with those of peptides **II** and **III**.

The conformational properties of the stereoisomeric peptides **4**−**11** were studied here in detail by using theoretical and spectroscopic (concentration- and temperature-dependent IR and NMR, solvent-dependent NMR and CD) analyses.

The prominent position of ferrocene in the field of medicinal chemistry is attributed to its unique properties (air and thermal stability, superaromaticity, electrophilicity, solubility in organic solvents, easy functionalization, nontoxicity, and lipophilicity).[28] Replacing the alkyl/aryl/heterocycle moiety of biologically active molecules with ferrocene or inserting ferrocene into an organic moiety/drug/drug-like molecule is a widely used method to develop efficient and selective anticancer, antioxidant, antituberculosis, antimalarial, anti-inflammatory, and antimicrobial therapeutics.[29,30] Since the first report of anticancer activity of a ferrocene derivative in 1978,[31] ferrocene compounds have been studied as potential anticancer, antibacterial, antifungal, and antiparasitic agents.[32,33] An overview of the antitumor activity of the ferrocifen family against breast cancer cells MCF-7 and MDA-MB-231 was given by Jaouen et al.[34]

In a recent review of the anticancer activity of ferrocene conjugated with various biomolecules, ferrocene conjugates with amino acids and peptides were highlighted as promising candidates for the development of new anticancer drugs due to their ability to overcome multidrug resistance during chemotherapy and to bind to specific receptors on cancer cells.[35] In terms of antibacterial capacity, highly potent antibacterial ferrocene-peptide conjugates have been reported to integrate into the bacterial membrane, leading to the detachment of vital enzymes required for respiration and cell wall biosynthesis.[36] The ferrocene group has also been used to modify and improve the activity of natural antioxidants.[37,38]

Considering the need to develop new efficient therapeutics for the treatment of infectious diseases, the ferrocene peptides **4**−**11** were subjected to an evaluation of their antitumor, antimicrobial, and antioxidant activities.

RESULTS AND DISCUSSION

Synthesis of Ferrocene-Containing Peptides 4−11. We have reported in a previous work the synthesis of ferrocene conjugates with L−Ala−L−Pro (**4** and **8**) and D−Ala−L−Pro (**5** and **9**), which were precursors of the homo- and heterochiral ferrocene peptides Ac−Ala−Pro−Fn−Pro−Ala−Boc.[14] The same simple and efficient strategy was applied to the synthesis of their enantiomers containing D−Ala−D−Pro (**7** and **11**) and L−Ala−D−Pro (**6** and **10**) (Scheme 1).

The starting fully protected ferrocene amino acid **1**[39] was Boc-deprotected by exposure to gaseous HCl, and the hydrochloride salt obtained was treated with an excess of NEt_3 to give the free *N*-terminus, followed by coupling with activated Boc−L−Pro−OH or Boc−D−Pro−OH to give the enantiomeric peptide **2** or **3**, respectively. Introduction of the L− and D−Ala units followed the Boc-deprotection of **2** and **3** as described above to give stereoisomeric peptides **4**−**7**. The bulky Boc-groups of carbamates **4**−**7** were replaced with sterically less demanding Ac groups upon (*i*) Boc-deprotection and (*ii*) Ac-protection in the presence of acetyl chloride to give acetamides **8**−**11**. The characterization data with IR, NMR, and MS spectra of new compounds **3**, **6**, **7**, **10**, and **11** can be found in the Supporting Information (Figures S1−S67).

In the following sections, we will analyze the conformational and biological properties of peptides **4**−**11**. Within the conformational analysis, the agreement between theoretically predicted and experimentally determined HB patterns of the targeted peptides was evaluated. Experimental spectroscopic analysis was performed for the new conjugates **6**, **7**, **10**, and **11**.

https://doi.org/10.1021/acs.organomet.4c00248
Organometallics 2024, 43, 2608−2625

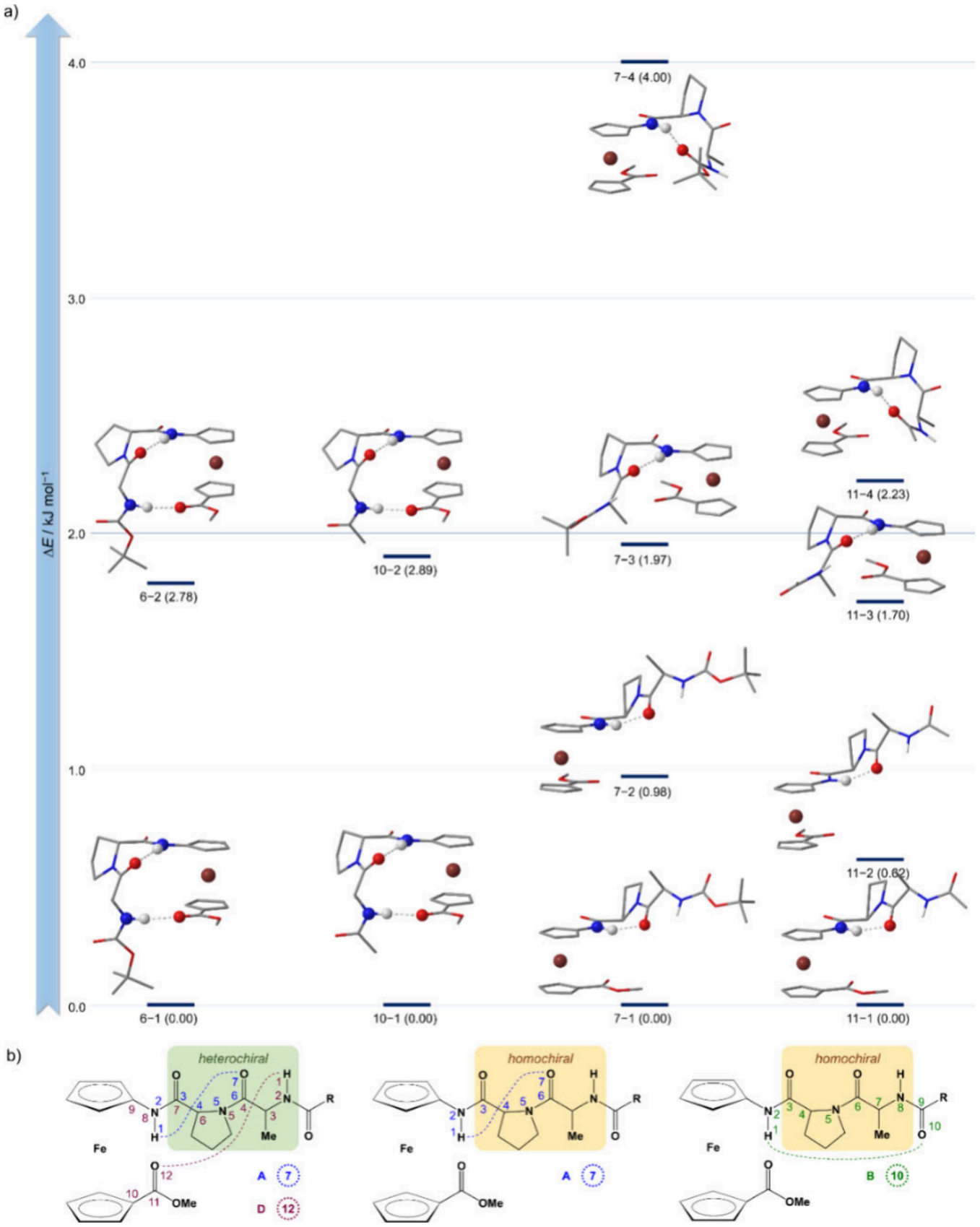

Figure 2. (a) DFT-optimized geometries (relative energies in kJ mol^{-1} in parentheses) of the most stable conformers of heterochiral (**6** and **10**) and homochiral peptides (**7** and **11**). Dashed lines represent hydrogen bonds verified by the QTAIM analysis. Nonpolar hydrogen atoms are omitted for clarity. (b) IHB patterns of the most stable conformers.

https://doi.org/10.1021/acs.organomet.4c00248
Organometallics 2024, 43, 2608−2625

Table 1. Relative Energies (Refer to Standard Gibbs Free Energies at 298 K in kJ mol^{-1}) of the Most Stable Conformers: Heterochiral Peptides 6 and 10 and Homochiral Peptides 7 and 11[a]

type	stereochemical descriptors	ΔE/ kJ mol^{-1}	ω/deg pseudotorsion angle	IHBs pattern	$NH_{Fn}\cdots OC_{Ala}$ 7-membered	$NH_{Fn}\cdots OC_{Ac/Boc}$ 10-membered	$NH_{Ala}\cdots OC_{COOMe}$ 12-membered
6−1	M-1,1′	0.00	−72.2	A + D	2.83	-	3.00
6−2	M-1,1′	2.78	−70.7	A + D	2.82	-	3.00
10−1	M-1,1′	0.00	−71.0	A + D	2.83	-	3.00
10−2	M-1,1′	2.89	−71.6	A + D	2.82	-	2.99
7−1	P-1,1′	0.00	+19.2	A	2.85	-	-
7−2	M-1,1′	0.98	−28.7	A	2.85	-	-
7−3	P-1,2′	1.97	+37.4	A	2.85	-	-
7−4	M-1,1′	4.00	−27.2	C	-	3.06	-
11−1	P-1,1′	0.00	+18.0	A	2.85	-	-
11−2	M-1,1′	0.62	−26.6	A	2.85	-	-
11−3	P-1,2′	1.70	+37.6	A	2.85	-	-
11−4	M-1,1′	2.23	−27.1	C	-	2.97	-

[a]Helicities were determined from pseudo-torsion angles. Intramolecular hydrogen bond (IHB) patterns are labeled as in Figure 2. X−Y distances (in Å) of the selected X−H···Y hydrogen bonds connecting the n-membered rings.

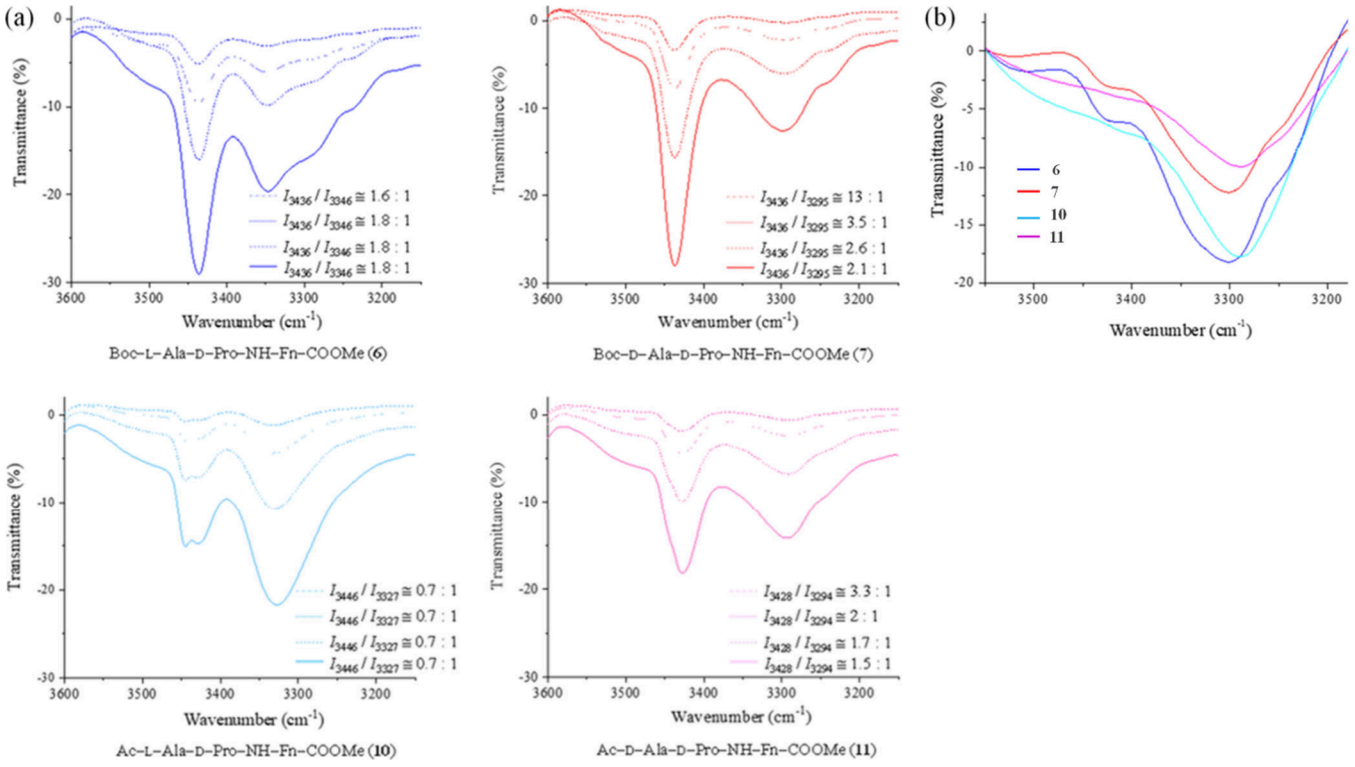

Figure 3. (a) The NH stretching vibrations in IR spectra of hetero-**6** and -**10** and homochiral ferrocene peptides **7** and **11** in CH_2Cl_2 [(—) $c = 5 \times 10^{-2}$ M, (- - -) $c = 2.5 \times 10^{-2}$ M, (● ● ●) $c = 1.25 \times 10^{-2}$ M, (- ● -) $c = 6.13 \times 10^{-3}$ and the ratios of the free and associated NH bands. (b) The NH stretching vibrations of compounds **6**, **7**, **10**, and **11** (2 mg) in KBr (200 mg).

Certainly, their enantiomers **4**, **5**, **8**, and **9**[16] were characterized by identical scalar properties.[40−42]

Computational Study. Computational chemistry methods can be a powerful tool for studying intermolecular interactions and HB patterns. Over the past decade, a hierarchical approach to conformational space analysis was used to study the conformational properties of monosubstituted and disubstituted ferrocene-based peptidomimetics,[14−16,20,43−47] the potential application of modified ferrocene-containing compounds as chirality sensors,[23,48,49] gellators,[50] and to better understand the relationship between the molecular structure of substituted ferrocene peptidomimetics and their biological activity.[15,16,19,51]

Previous conformational analysis showed that disubstituted derivatives Ac/Boc−Ala−Fn−COOMe (**I**) simultaneously form two hydrogen bonds, the first connecting the 7-membered intrastrand (pattern **A**) and the second connecting the 9-membered interstrand ring (pattern **B**) (Figure 1).[18] Incorporating Pro in place of Ala triggers the formation of a different HB pattern with only one 7-membered ring (pattern **A**).[19] We can divide their higher homologues Ac/Boc−Pro−Ala−Fn−COOMe (**III**)[15] into homochiral and heterochiral, depending on the chirality of alanine and proline. While the homochiral diastereomers form either a 9-membered interstrand (pattern **B**) or 10-membered intrastrand ring (pattern **C**), their heterochiral analogues mostly form conformers with

https://doi.org/10.1021/acs.organomet.4c00248
Organometallics 2024, 43, 2608−2625

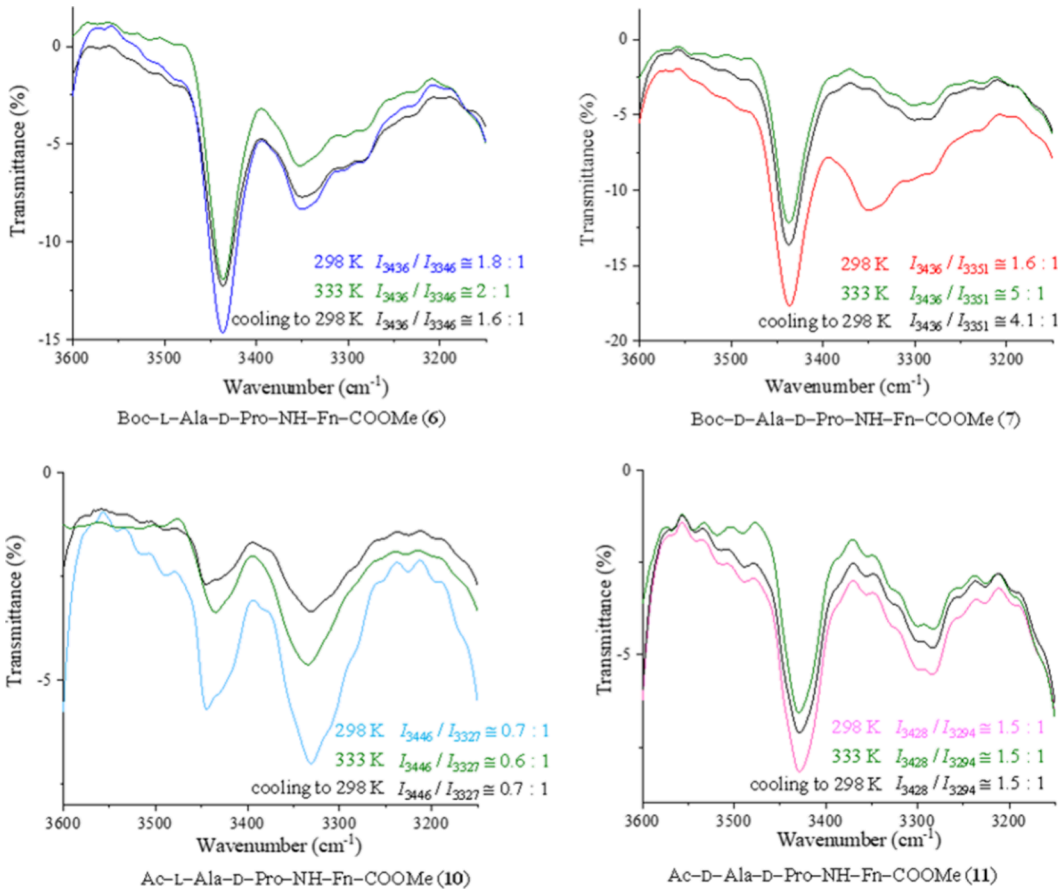

Figure 4. NH stretching vibrations in the temperature-dependent IR spectra of hetero-**6** and -**10** and homochiral ferrocene peptides **7** and **11** in $CHCl_3$ ($c = 5 \times 10^{-2}$ M) and the ratios of the free and associated NH bands.

all NH donors involved in HBs.[15] Therefore, in this article, we have investigated the effect of interchanged dipeptide sequences (Pro−Ala in **III** to Ala−Pro in **IV**) on the formation of HB patterns (Figure 2, Table 1).

The analysis was performed only on diastereomers **6**, **7** and **10**, **11**, but the same scalar properties are expected for their enantiomers **5**, **4** and **9**, **8**, respectively. By interchanging the positions of Ala and Pro, the position of one (NH_{Ala}) donor is shifted as well, while the other (NH_{Fn}) remains in the same position. Such shifting of NH groups initiated the formation of relatively strong 7-membered $N-H_{Fn}\cdots OC_{Ala}$ hydrogen-bonded rings (pattern **A**) in both diastereomers, heterochiral (**6** and **10**) and homochiral (**7** and **11**). However, the heterochiral sequence establishes a relatively tight structure in which another 12-membered interstrand ring connected by $N-H_{Ala}\cdots OC_{COOMe}$ hydrogen bonds is also formed (pattern **D**). In homochiral analogs, only one interstrand hydrogen bond persists, either $N-H_{Fn}\cdots OC_{Ala}$ or $N-H_{Fn}\cdots OC_{Ac/Boc}$, in a 7- (pattern **A**) or 10-membered ring (pattern **C**), respectively. Because of the interstrand hydrogen bond, the heterochiral derivatives **6** and **10** are locked into M- (L−Ala−D−Pro) or P-helical (D−Ala−L−Pro) configurations, while the absence of similar hydrogen bonds in homochiral **7** and **11** results in pairs of conformers differing mostly in pseudo-torsion angles (e.g., **7**−**1** and **7**−**2**). The results of the computational study indicated that the heterochiral Ala−Pro sequence in novel conjugates **IV** and the Pro−Ala sequence in **III**[15] promote the formation of tighter ferrocene-based peptide structures with both NH groups involved in HBs.

IR Spectroscopy. In contrast to NMR, the IR time scale is fast and allows discrimination between different conformations adopted by the same protein.[52,53] IR frequencies of backbone N−H and C═O groups depend on their participation in HBs and are red-shifted and enhanced when an N−H···O═C bond is formed.[54−57] The red-shifted stretching frequencies of NH (~3350−3240 cm^{-1}) and $CO_{Boc/Ac}$ groups (~1680−1660 cm^{-1}) indicate their involvement in hydrogen bonding[58−60] (Figure 3, see Supporting Information, Figures S9, S24, S39, and S54). However, judging from the ratio of free (>3430 cm^{-1}) and associated NH groups, Ac-peptides **10** and **11** are involved in hydrogen bonding to a greater extent than Boc-peptides **6** and **7**, which are dominated by nonbonded NH groups (Figure 3a). However, the predominance of hydrogen-bonded NH groups was observed in the solid state of the tested peptides (Figure 3b).

To determine whether the hydrogen bonding occurs in an intra- or intermolecular manner, we recorded the IR spectra of peptides **6**, **7**, **10**, and **11** at various concentrations (5×10^{-2}, 2.5×10^{-2}, 1.25×10^{-2}, and 6.13×10^{-3} M). If the HBs are intramolecular, then gradual dilution does not disturb the ratio of bonded and nonbonded NH bands. However, if the intensity of the associated NH bands decreases upon dilution compared to that of the free NH bands, then this suggests the presence of intermolecular aggregates. Because the ratio of free and associated NH bands of peptides **7** and **11** is increased upon dilution by 40−60%, the molecules of these homochiral derivatives partially participate in intermolecular HBs (Supporting Information, Figures S25 and S55). In contrast,

https://doi.org/10.1021/acs.organomet.4c00248
Organometallics 2024, 43, 2608−2625

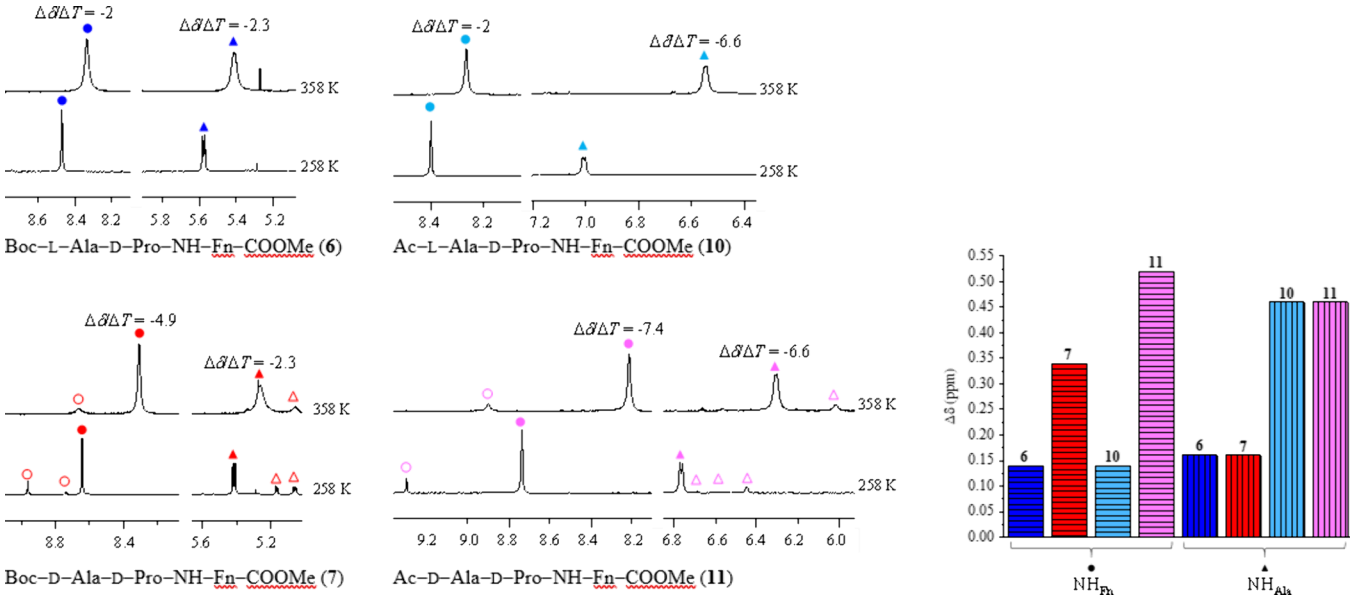

Figure 5. Changes in chemical shifts ($\Delta\delta$) of NH_{Fn} (●) and NH_{Ala} (▲) in hetero-**6** and -**10** and homochiral ferrocene peptides **7** and **11** in $CDCl_3$ ($c = 1 \times 10^{-3}$ M) from 258 to 328 K. The *cis*/*trans* isomerization in homochiral peptides **7** and **10** ($NH_{Fn\ trans}$ (●), $NH_{Ala\ trans}$ (▲), $NH_{Fn\ cis}$ (○), and $NH_{Ala\ cis}$ (Δ)). The NH stretching vibrations in the temperature-dependent IR spectra of hetero-**6** and -**10** and homochiral ferrocene peptides **7** and **11** in $CHCl_3$ ($c = 5 \times 10^{-2}$ M) and the ratios of the free and associated NH bands.

the heterochirality of peptides **6** and **10** may be responsible for their engagement only in intramolecular HBs, as suggested by the almost unchanged ratio of free and associated NH bands (Supporting Information, Figures S10 and S40). In addition, we were interested in investigating whether temperature affects the HB patterning of the peptides studied.[61,62] Temperature-dependent IR spectra were recorded in $CHCl_3$ at 293 K, after heating to 333 K and gradual cooling to 293 K (Figure 4). For the homochiral Ac-peptide **11**, for which the intermolecular hydrogen bonding was predominant, no change in the ratio of free and associated NH bands was observed. For heterochiral peptides **6** and **10**, the effect of temperature on the pattern of NH bands was only slight, and after cooling to room temperature, the pattern of NH bands was restored. The obtained results indicate that **6**, **10**, and **11** adopt stable hydrogen-bonded structures. In contrast, temperature was found to allow tuning of the HB pattern of homochiral Boc-peptide **7**. Its associated NH band at 3351 cm^{-1} almost disappeared in favor of the free NH band at 3436 cm^{-1}, whose intensity was increased by up to 3-fold. The observed dominance of the free NH band persisted after cooling to 293 K. The frequencies of the overlapped CO stretching vibrations (1800−1600 cm^{-1}) of the tested peptides were not shifted at higher temperatures (Supporting Information, Figures S11, S26, S41, and S56).

NMR Spectroscopy. NMR spectroscopy is widely used to provide information on the structure of small peptides that are prone to conformational changes[63] and on the interactions of peptides and proteins to identify bioactive conformations responsible for drug-like properties.[64] In this study, we have used a detailed NMR analysis (^1H, ^{13}C, $^1H-^1H$ COSY, $^1H-^1H$ NOESY, $^1H-^{13}C$ HMQC, and $^1H-^{13}C$ HMBC) for the assignment of individual proton resonances and the determination of HB patterns for the peptides under study. [For the full NMR characterization, please refer to the Supporting Information, Figures S1−S6 (**3**), S13−S18 (**6**), S28−S33 (**7**), S43−S48 (**10**), and S58−S63 (**11**).]

Due to the deshielding that occurs in the hydrogen bonds, the resonances of the amide protons involved in the HBs are moved downfield ($\delta \geq 7$ ppm) in the nonpolar $CDCl_3$,[65,66] and the greater downfield shifting is related to the stronger HBs.[67] Therefore, it is expected that the NH_{Fn} protons, whose resonances are downfield-shifted ($\delta \approx 8.4$ ppm), are involved in the HBs, while the upfield-shifted resonances of NH_{Ala} protons ($\delta \approx 6.6$ ppm) in Ac-peptides **10** and **11** could be attributed to their somewhat limited hydrogen-bonding capacity. This could also be true for the NH_{Ala} protons in Boc-peptides **6** and **7**, whose upfield-shifted resonances ($\delta \approx$ 5.4 ppm) are influenced by the chemically different character of the urethane unit in the Boc-terminal group[68] (Figure 5 and Figures S13, S28, S43 and S58 in the Supporting Information).

Further insight into the conformational properties of peptides **6**, **7**, **10**, and **11** was gained by examining the concentration dependence, temperature dependence, and solvent dependence of their NH chemical shifts.

Since the IR spectra of homochiral peptides **7** and **11** were concentration-dependent, indicating the presence of intermolecular aggregates, we expected a broadening and upfield shifting of the NH signals at dilutions of up to 50-fold,[67] but instead only the slightly impaired resonances were observed. The chemical shifts of the NH protons of heterochiral peptides **6** and **10** were also independent of concentration (Supporting Information, Figures S19, S34, S49, and S64), suggesting the presence of IHBs.

Next, the stability of the intramolecularly hydrogen-bonded structures was investigated by measuring the temperature dependence of the chemical shift of the amide protons in the range of 258−328 K, and the smaller the shifts, the more stable the hydrogen-bonded conformations. When the sharper peaks are observed at low temperatures, the molecules also move more slowly.[63,69] Here, the heterochiral Boc-peptide **6** was proven to adopt the most stable IHB pattern ($\Delta\delta$ (NH_{Fn}, NH_{Ala}) < 0.15 ppm) compared to those of the other peptides tested, which agrees well with its temperature-independent IR

https://doi.org/10.1021/acs.organomet.4c00248
Organometallics 2024, 43, 2608−2625

data. The upfield shifting of signals belonging to the NH_{Fn} of peptide **7**, NH_{Ala} of peptide **10**, and NH_{Fn} and NH_{Ala} of peptide **11** ($\Delta\delta \approx 0.35-0.55$ ppm) at increased temperature suggests that these protons may be involved in more flexible HB patterns (Figure 5).

The variations in the chemical shifts of the amide protons with temperature (temperature coefficients, $\Delta\delta/\Delta T$), provide further information about hydrogen bonding. The low $\Delta\delta/\Delta T$ values (-2.4 ± 0.5 ppb K^{-1}) correspond to either shielded protons which were initially downfield shifted or protons exposed to $CDCl_3$ and are therefore not informative in defining the hydrogen-bonding pattern. In contrast, the larger $\Delta\delta/\Delta T$ values always reflect NH protons that were initially shielded from the solvent but are exposed during the unfolding of the IHB pattern or the dissociation of intermolecular aggregates upon heating.[14−17,70−78] Here, the larger temperature coefficients observed for NH_{Fn} and NH_{Ala} of peptide **11** and NH_{Fn} of peptide **7**, whose IR frequencies were concentration-dependent, provide additional confirmation of their aggregation tendency, while the case of the concentration-independent NH_{Ala} of peptide **10** reflects its involvement in IHB-mediated folding. This is in good agreement with the results of the computational study where heterochiral derivatives **6** and **10** have both NH donors involved in hydrogen bonding.

The slow *cis*/*trans* isomerization of the proline imide bond leads to multiple signals of the amide protons in the NMR spectra. Upon heating, the isomerization rate increases, causing the coalescence of the signals of the amide protons involved in weak hydrogen bonds.[72,79,80] Here, the multiple signals observed for homochiral peptides **7** and **11** at low temperatures tend to coalesce at higher temperatures, which can be considered to be additional evidence for their involvement in weak hydrogen bonds (Figure 5 and Figures S20, S35, S50, and S65 in the Supporting Information).

IR and NMR data indicate the flexible IHB patterning of homochiral peptides **7** and **11**, whereas heterochiral peptides **6** and **10** adopt the more stable structures in nonpolar solvents ($CHCl_3$ and $CDCl_3$). The same results for the contribution of heterochirality to conformational stability were also found in our previous work. Their constitutionally isomeric peptides **III** with heterochiral Pro−Ala sequences[15] and disubstituted conjugates of ferrocene-1,1′-diamine with heterochiral Ala−Pro sequences[14] were also shown to adopt more stable IHB-based structures than homochiral analogs.

It is well known that a strong hydrogen-bonding solvent such as DMSO solvates exposed amide protons, leading to a pronounced downfield shifting and opening of the flexible structures.[14,68,81] The appreciable downfield shifting of the NH_{Ala} groups observed here upon titration with DMSO ($\Delta\delta \approx 1.2-1.6$) is attributed to a high solvent sensitivity due to the noninvolvement in HBs or involvement in only weak HBs. Similarly, the relatively high solvent sensitivity of downfield-shifted NH_{Fn} groups of conjugates **7** and **11** ($\Delta\delta \approx 0.9$) supports the assumption of flexible IHB patterns in homochiral peptides. For the NH_{Fn} of heterochiral peptides **6** and **10**, the slope of the titration curve is smaller ($\Delta\delta < 0.5$) than that of homochiral peptides **7** and **11**, indicating that heterochirality of the peptide backbone contributes to more stable IHB patterns, as suggested above (Figure 6).

As for the *cis*−*trans* isomerization of a proline imide bond in small peptides, nonpolar solvents and IHBs were found to contribute to the prevalence of the *trans* fraction.[82,83] While

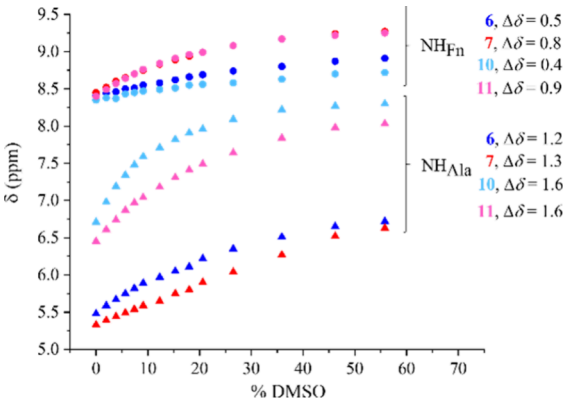

Figure 6. Changes in chemical shifts ($\Delta\delta$) of NH_{Fn} (●) and NH_{Ala} (▲) in hetero-**6** and -**10** and homochiral ferrocene peptides **7** and **11** at increasing concentrations of d_6-DMSO in $CDCl_3$ (c = 25 mM, 298 K).

only *trans* isomers were observed in the nonpolar $CDCl_3$ solution of heterochiral peptides **6** and **10**, their titration with DMSO caused the appearance of additional peaks of NH groups assigned to their *cis* fractions. The observed doubling of amide resonances of heterochiral peptides **6** and **10** upon titration with DMSO suggests that they are involved in IHBs of only moderate strength (Figure 6 and Figures S21, S36, S51, S66, and S67 in the Supporting Information).

Two-dimensional NOESY spectroscopy was used to gain better insight into the IHB patterning of the peptides studied. Considering the possible interactions between hydrogen-bond-donating and -accepting groups, we focused on the intrastrand NOE interactions between NH_{Fn} and the protons of the Ala moiety and on the interstrand NOE interactions between NH_{Fn} and NH_{Ala} with the ester methyl group.

Although the temperature dependence and DMSO dependence of NH chemical shifts of the homochiral peptides revealed that their HB patterns are more sensitive and weaker than those of the heterochiral analogs, their common conformational feature is based on the IHB engagement of the NH_{Fn} protons. The observed intrastrand NOE contacts $NH_{Fn} \rightarrow Ala-CH_3$ and $NH_{Fn} \rightarrow Ala-CH$ might account for the 7-membered IHB ring (γ-turn, pattern **A**) (Figure 7).

CD Spectroscopy. To further examine the conformational consequences of HB-mediated folding in ferrocene peptides, we performed circular dichroism analysis (CD).[84,85] The folding of ferrocene peptides into turn- and β-sheet-like structures fairly restricts the free rotation of the cyclopentadienyl rings. This leads to a helical chirality of the ferrocene core which can be registered by Cotton effects in the region of ferrocene-based transitions around 470 nm. When the folded conformations are more stable, the Cotton effects are of higher intensity. The Cotton effects with lower intensity were registered for the structures with hydrogen bonding within the same strand, indicating the presence of the less stable conformations.[15,18,19,46] In general, the reduction of hydrogen bonding leads to more flexible structures and the CD activity decreases. Moreover, the positive or negative sign of the Cotton effect is related to the right- or left-handed helicity of the ferrocene core.[86]

Since the IR and NMR data support the involvement of the heterochiral peptides **6** and **10** containing the Ala−Pro sequence in IHBs of only moderate strength, their Cotton effects are ~20-fold weaker than those of their heterochiral

https://doi.org/10.1021/acs.organomet.4c00248
Organometallics 2024, 43, 2608−2625

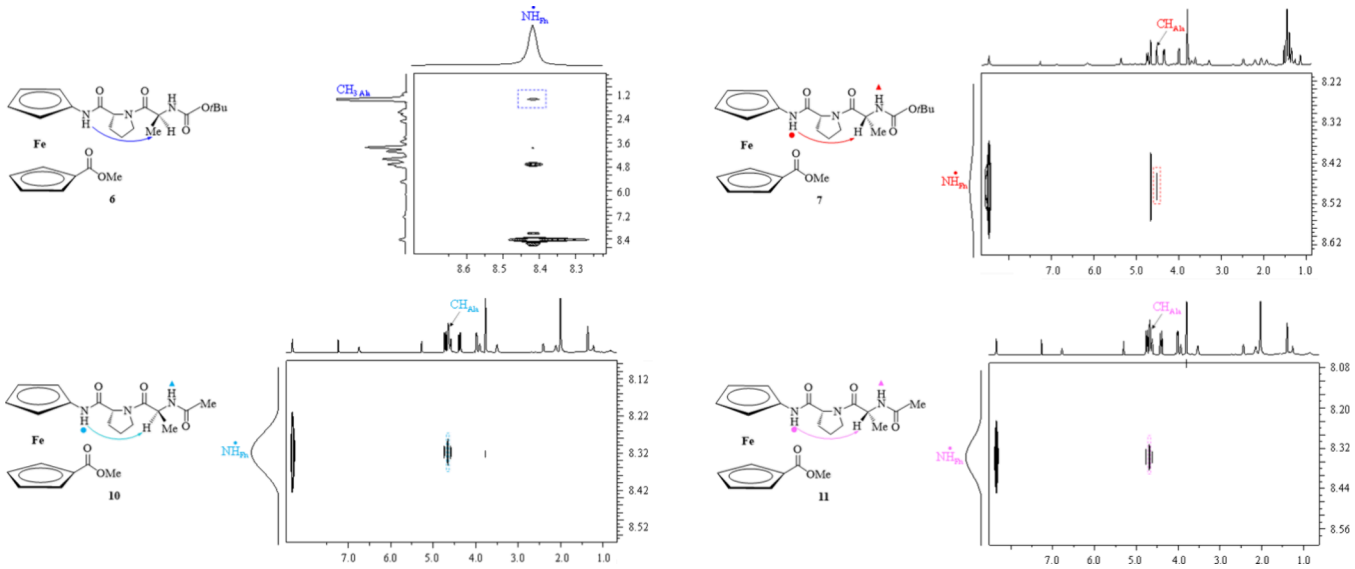

Figure 7. Intrastrand NOE contacts in the spectra of heterochiral **6** and **10** and homochiral ferrocene peptides **7** and **11** depicted with arrows.

counterparts **III**[15] with a Pro−Ala sequence ($M_\theta \approx 4200-4800$ deg cm^2 dmol^{-1}), which were found to be involved in strong IHBs. In general, novel peptides **IV** (**4**−**11**) showed a significant decrease in CD activity ($M_\theta \approx 100-800$ deg cm^2 dmol^{-1}) compared with their constitutional isomers **III** with an exchanged dipeptide sequence ($M_\theta \approx 2500-4800$ deg cm^2 dmol^{-1}) (Figure 8). The CD activity results suggest that the presence of proline next to the ferrocene moiety in the novel peptides **IV** hinders the formation of stable-turn structures, whereas the insertion of alanine between ferrocene and proline enables the folding of the peptides **III** into more stable turns.

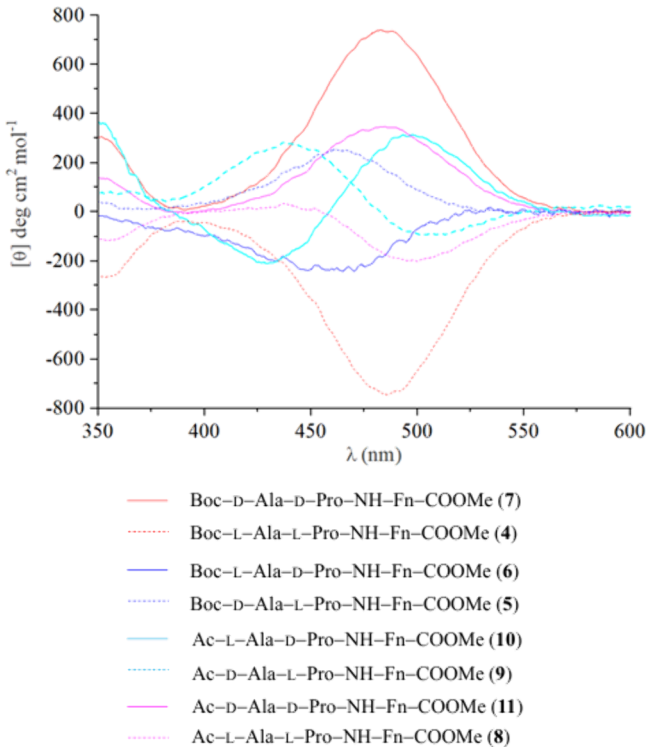

Figure 8. Cotton effects of ferrocene peptides **4**−**11** in CH_2Cl_2 ($c = 1 \times 10^{-3}$ M).

X-ray Crystal Structure Analysis. Compound **3** is a D-enantiomer of a previously published compound[19] and is therefore not described in detail (Figure 9a). Compound **4**

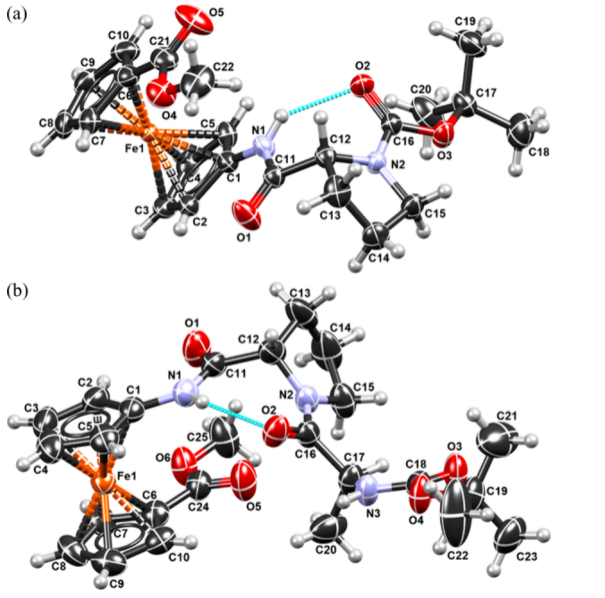

Figure 9. Drawings of molecules **3** (a) and **4** (b) with atom numbering schemes. Displacement ellipsoids are drawn for the probability of 50%, and hydrogen atoms are shown as spheres of arbitrary radii. IHBs are shown as cyan dotted lines.

crystallizes in the tetragonal system, space group P 41212, with one symmetry-independent molecule (Figure 9b). Its conformation is stabilized by a single intramolecular hydrogen bond, N1−H1···O1, so it belongs to pattern type **A** (7-membered ring, i.e., γ-turn). By a pair of symmetry-equivalent intermolecular hydrogen bonds N3−H3···O2, the molecules are linked into a centrosymmetric dimer; these dimers are connected by C−H···O hydrogen bonds into a 3D network.

The molecular structure of peptide **4** determined by X-ray crystallography corresponds to the third conformer obtained by DFT analysis of its enantiomeric pair **7** (**7**−**3** and **4**−**3** are

https://doi.org/10.1021/acs.organomet.4c00248
Organometallics 2024, 43, 2608−2625

mirror images) with an RMSD value of 0.3294 Å (Figure S68 in the Supporting Information). Although the same IHB pattern **A** is observed in all three conformers of **7** (**7−1**, **7−2**, and **7−3** and their enantiomers **4−1**, **4−2**, and **4−3**), the possible explanation of why the most stable conformers are not observed in the solid state is due to the more likely orientation of the HB donors and acceptors to form intermolecular hydrogen bonds. The energy input required for the reorganization from the most stable conformer (**4−1**) to the less stable one (**4−3**) is overcome by the energy gain from the intermolecular hydrogen bonding of the molecules in the centrosymmetric dimer. We have already explained this effect by evaluating interaction energies in similar systems.[53]

Biological Activity. The achievements in the field of ferrocene-modified compounds with potential in vitro and in vivo biological activities, including anticancer, antifungal, antimalarial, and anticoronaviral activities, have been recently reviewed.[87] The introduction of ferrocene-modified amino acids has been shown to cause the changes in synaptic transmission in the CA1 region of the hippocampus. More specifically, the introduction of ferrocene-containing compounds led to an increase in the amplitudes of local field potentials, and the hippocampus responded differently to electrical signals when ferrocene-modified L- and D-amino acids were administered in vivo (rats).[88] This indicates that the presence of the ferocene group can improve the biological activity of ferrocene-modified amino acids.

Antimicrobial Activity. According to the results of the conducted disc diffusion test, the tested ferrocene conjugates with Ala−Pro (**4−11**) were not effective in inhibiting the growth of the tested microorganisms. No zones of inhibition were observed around the diagnostic discs, indicating the resistance of the tested bacteria, lactic acid bacteria, and yeasts to these ferrocene tripeptides (data not shown). No difference in survival was observed before and after treatment with the tested peptides at concentrations of 2 and 4 mM, although an increase in the solubility of poorly water-soluble compounds by mixing with methyl-β-cyclodextrin has been reported in the literature.[89] The tested ferrocene peptides did not exhibit antimicrobial activity, although the significant antimicrobial activity of proline-rich AMPs has been reported in the literature, mainly through nonlytic mechanisms.[90]

In our recent work, we reported the biological evaluation of enantiomeric dipeptides derived from 1′-aminoferrocene-1-carboxylic acid and the hydrophobic amino acids Leu and Phe, which exhibited antimicrobial activity against *P. aeruginosa*, *B. subtilis*, and *S. aureus* at a concentration of 2 mM.[16] These results may be related to the fact that antimicrobial peptides containing Leu or Phe as the only hydrophobic groups bind bilayers with the highest affinity and are most effective at inhibiting bacterial growth due to their greater ability to disrupt bacterial membranes.[91] Peptides containing Val showed low antimicrobial activity and ability to interact with bilayers,[92] which is consistent with our previous results.[16] In contrast to these results, the homochiral conjugates of ferrocene-1,1′-diamine with L−/D−Phe, L−/D−Val, and L−/D−Leu described in our recent paper,[16] as well as the compounds **4−11** tested in this work, unfortunately showed no antimicrobial activity despite the high concentrations applied (153−251 mM).

Antiradical Activity. According to Zhang et al.,[93] proline is an amino acid with relatively strong ROS scavenging activity. Therefore, the antiradical activity of the proline-containing bioconjugates **4−11** was estimated using assays for determining the ability of the compounds to scavenge free radicals: 2′-diphenyl-1-picrylhydrazyl radical (DPPH) and 2,2′-azinobis(3-ethylbenzothiazoline-6-sulfonate) cationic radical (ABTS). The results of the free radical scavenging activity of the tested compounds, expressed as mM Trolox equivalents, are shown in Figure 10. The tested compounds (1 mM) showed very similar

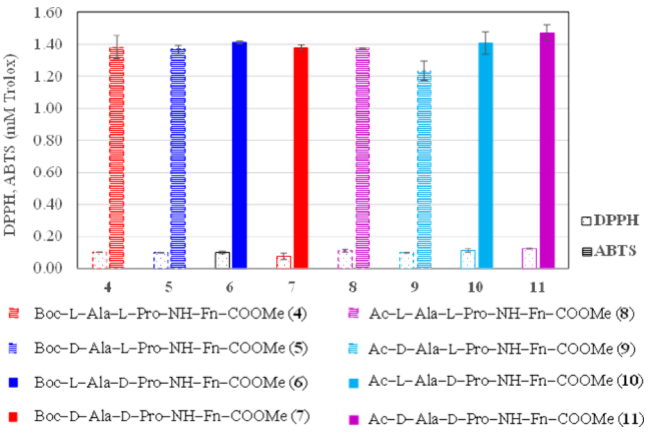

Figure 10. Antiradical activity of bioconjugates **4−11** evaluated by using the free 1,1-diphenyl-2-picryl hydrazyl radical scavenging assay (dot) and the ABTS radical cation scavenging assay (line).

antiradical activity against both DPPH and ABTS radicals in the ranges of 0.08−0.12 and 1.23−1.47 mM Trolox, respectively. These results suggest that the chirality of the Ala−Pro sequence in bioconjugates **4−11** does not significantly affect the antiradical activity.

The influence of the protecting group type (Boc or Ac) on the antiradical activity of the tested compounds was also not observed. The tested ferrocene compounds showed better scavenging activity against ABTS radicals than against DPPH radicals. This is consistent with literature data suggesting that ferrocene derivatives are more active with reducing radicals (such as $ABTS^{\bullet+}$) than with donating radicals (such as $DPPH^{\bullet}$),[94] whose steric availability is critical for antioxidant activity.[95] The antioxidant activity of peptides **4−11** is lower than that of known natural antioxidants such as red and white wine,[96] strawberries and blackberries, and coffee.[97] However, the antioxidant activity of peptides **4−11** is similar to that of tomato processing byproducts in the food industry (about 0.25 mmol Trolox/g in the DPPH assay and about 1.0 mmol Trolox/g in the case of the ORAC assay).[98] Considering that food industry byproducts have been shown to be valuable sources of antioxidants,[110] we believe that ferrocene bioconjugates **4−11**, which have similar antioxidant potentials, could serve in the further development of more effective antioxidants.

Antiproliferative Activity. Several ferrocene-based compounds have shown significant *in vitro* activity in various cell lines[34,54,99] and are therefore promising for the development of novel therapeutics for a wide range of diseases, including cancer.[100] Recent studies have shown that compounds modified with ferrocene can induce cell death in cancer cells, leading to their selective elimination.[98,101] For example, the cytotoxic potential of two ferrocene-containing camphor sulfonamides was studied in nonsmall lung cancer (A549 and H1299) and in a noncancerous cell line (MRC5). The results were significantly lower IC_{50} values, of about 12 to 22 μM in

https://doi.org/10.1021/acs.organomet.4c00248
Organometallics 2024, 43, 2608−2625

A549 and H1299 cancer cells, which is even lower than for reference antitumor drugs cisplatin and tamoxifen.[98] Also, a series of 2-acyl-1-dimethylaminomethyl-ferrocenes have been evaluated against T cell acute lymphoblastic leukemia (T-ALL) cell lines as a potential cancer therapy. These novel ferrocene derivatives also exhibit significantly lower IC_{50} values, ranging from about 18 to 44 μM in three cancer cell lines (Jurkat, CEMT4, and Molt-4). At the same time, the tested compounds displayed low cytotoxicity in normal cells (normal human T and HEK293), encouraging the clinical application of derivatives F1 and F3 for the treatment of T-ALL.[97]

In this work, the antiproliferative activity of compounds **4**–**11** was investigated in a concentration range from 50 to 500 μM in the human tumor HeLa cell line. The results for D-proline-containing peptides **6**, **7**, **10**, and **11** and their enantiomers **5**, **4**, **8**, and **9**, respectively, containing L-proline are shown in Figure 11a,b, whereas the calculated IC_{50} values are given in Table 2.

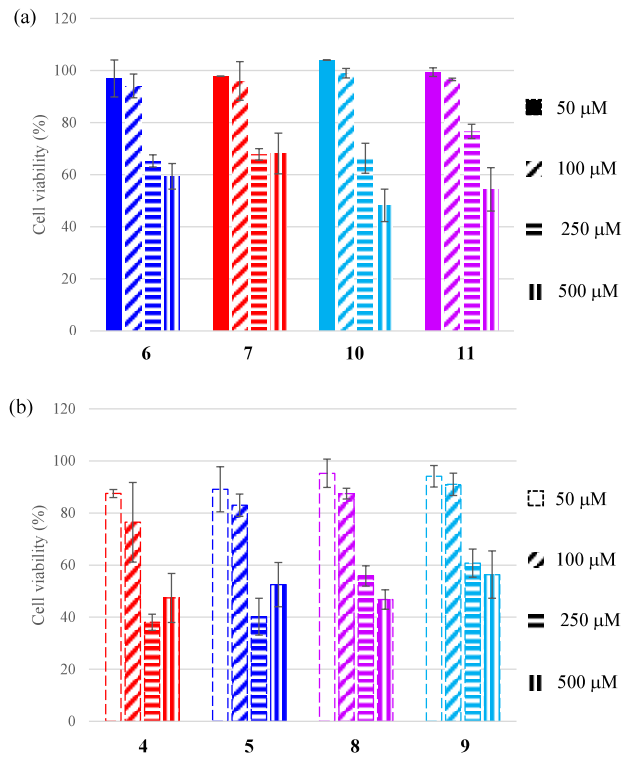

Figure 11. Antiproliferative activity of (a) bioconjugates **6**, **7**, **10**, and **11** and (b) their enantiomers **4**, **5**, **8** and **9** evaluated by CellTiter 96 AQueous One Solution Cell Proliferation assay on HeLa cells. Data show the mean ± SD of n = 3 independent experiments.

Table 2. IC_{50} Values Calculated from Dose–Response Curves on HeLa Cells

Compound	IC_{50} (μM)
Boc–L–Ala–L–Pro–NH–Fn–COOMe (**4**)	238.62
Boc–D–Ala–L–Pro–NH–Fn–COOMe (**5**)	353.62
Boc–L–Ala–D–Pro–NH–Fn–COOMe (**6**)	n.d. (>500)
Boc–D–Ala–D–Pro–NH–Fn–COOMe (**7**)	n.d. (>500)
Ac–L–Ala–L–Pro–NH–Fn–COOMe (**8**)	401.67
Ac–D–Ala–L–Pro–NH–Fn–COOMe (**9**)	n.d. (>500)
Ac–L–Ala–D–Pro–NH–Fn–COOMe (**10**)	493.17
Ac–D–Ala–D–Pro–NH–Fn–COOMe (**11**)	533.24

The bioconjugates tested showed moderate growth inhibition in HeLa cells, mostly at higher concentrations tested (250 and 500 μM). Among the D-proline-containing bioconjugates, similar growth inhibition of HeLa cells was observed, and Ac-peptides **10** and **11** exhibited slightly higher cytotoxicity than Boc-analogues **6** and **7**, with calculated IC_{50} values of 493.17 and 533.24 μM, respectively. As for the L-proline-containing enantiomers, Boc-peptides **4** and **5** showed a somewhat higher inhibitory activity than Ac-analogues **8** and **9**, with IC_{50} values of 238.62 and 353.62 μM, respectively. Our previous studies on ferrocene peptides[13,15,16] have shown that lipophilicity affects biological activity more than conformational patterning. Thus, the slightly stronger antiproliferative activity of Boc-peptides **4** and **5** can be attributed to their higher lipophilicity (i.e., they have larger retention factors ($R_f \approx 0.3$–0.6) than Ac-peptides **8**–**11** ($R_f \approx 0.05$–0.15) (dichloromethane:ethyl acetate = 5:1)).

However, our previous studies showed the more pronounced cytotoxic effect on HeLa cells for their lower Boc-homologue **II** (IC_{50} = 203.27 μM),[19] while the slightly enhanced inhibitory potential was observed for their constitutionally exchanged counterparts **III** (IC_{50} = 370.39 and 436.20 μM).[15] Thus, the structural and conformational modulation of the peptides **II** and **III** to the novel peptides **IV** (**4**–**11**) did not improve their inhibitory activity.

The cytotoxicity observed for the tested peptidomimetics may stem from their effects on fundamental cellular processes, specifically cell division and cell death. Programmed cell death via apoptosis was evaluated and quantified by flow cytometry analysis using the Muse Cell Analyzer and the Muse Annexin V and Dead Cell Kit. The results of this analysis for HeLa cells are presented in the Supporting Information (Figure S69).

In this assay, only compounds with IC_{50} values below 500 μM were tested. The results of the analysis showed that HeLa cells treated with compounds **4** and **5** had the highest percentage of total apoptotic cells (36.21 ± 6.28 and 35.99 ± 6.83%, respectively), followed by compounds **8** and **10**. The results of the analysis of cell death in the treated HeLa cells are consistent with the cell viability assay used primarily to assess the basic cytotoxicity of the peptides **4**–**11**. The induction of apoptosis by the action of peptidomimetics has been reported previously,[102] whereby peptidomimetics with anticancer properties bind to target proteins and mimic interactions that activate death pathways in cancer cells. Peptidomimetics often act as inhibitors of protein–protein interactions in cancer cells, as recently highlighted by Mabonga et al.[103]

Finally, according to the U.S. National Cancer Institute (NCI) and its in vitro primary screening panel of 60 different human tumor cell lines,[104] the tested bioconjugates **4**–**11** have low antiproliferative activity against HeLa cells, as all IC_{50} values obtained are above 100 μM. Therefore, they cannot be considered to be potential anticancer drug candidates but could rather serve as a guide for the rational design and further development of new ferrocene bioconjugates with improved biological activity.

CONCLUSIONS

This research is a small step toward building a small database of relatively simple ferrocene-based peptidomimetics and investigating the relationship among their structures, conformational properties, and biological activities. Compared to the previously reported lower homologues with only one amino acid, the higher Ac/Boc–Ala–Pro–Fn–COOMe

https://doi.org/10.1021/acs.organomet.4c00248
Organometallics 2024, 43, 2608–2625

homologues occur as heterochiral or homochiral diastereomers. Conformational analysis showed that heterochiral derivatives form tighter structures in which both NH hydrogen-bond donors are involved in hydrogen bonding. Compared with the results of previous studies (Ac/Boc−Pro−Ala−Fn−COOMe), the relatively simple exchange of the dipeptide sequence from Pro−Ala to Ala−Pro also resulted in a change in the main structural motif from a ten- to a seven-membered intrastrand hydrogen-bonding ring. Although the tested derivatives showed limited biological activity, the current study based on joint experimental and computational techniques gave us the opportunity to focus on the structure−activity relationship. We have shown that small structural changes, such as changing the order of two amino acids, not only alter the organizational level of dipeptide attached to the ferrocene core and thus the related conformational properties but also can affect the antimicrobial, antiradical, and antiproliferative activity of the compounds studied.

EXPERIMENTAL SECTION

Materials and Methods. *General Procedures and Methods.* We have reported the synthesis of peptides containing L−Ala−L−Pro (**4** and **8**) and D−Ala−L−Pro (**5** and **9**) in a previous work,[14] and the same simple and efficient strategy was applied here to the synthesis of their enantiomers with D−Ala−D−Pro (**7** and **11**) and L−Ala−D−Pro (**6** and **10**) (Scheme 1). All reactions were carried out under an argon atmosphere, and chemicals used for reactions were analytically pure. The CH_2Cl_2 used for CD measurements and FTIR was dried (P_2O_5), distilled over CaH_2, and stored over molecular sieves (4 Å). $CDCl_3$ and DMSO-d_6 (Sigma-Aldrich), EDC (Acros Organics), HOBt (Aldrich), acetyl chloride (Aldrich), Boc−D−Ala−OH (Fisher), H−D−Pro−OH (Biosynth), H−L−Pro−OH (Acros Organics), and L-alanine (Merck) were used as received. The synthesis of Boc−NH−Fn−COOMe (**1**) had been previously described.[38] The *N*-termini of alanine and proline were protected by using sodium hydroxide, aqueous dioxane, and di-*tert*-butyldicarbonate to give Boc−Ala−OH, Boc−D−Pro−OH, and Boc−L−Pro−OH, respectively. Products were purified by preparative thin layer chromatography on silica gel (Merck, Kieselgel 60 HF_{254}) by using CH_2Cl_2, EtOAc, or a EtOAc/CH_2Cl_2 mixture as the eluent. Infrared spectra were recorded as CH_2Cl_2 or $CHCl_3$ solutions between NaCl windows or in KBr by using a Spectrum Two FTIR spectrometer (PerkinElmer); [(s) = strong, (m) = medium, (w) = weak, (br) = broad, (sh) = shoulder]. NMR spectra were recorded using a Bruker AV600 spectrometer (Bruker BioSpin GmbH, Rheinstetten, Germany) with a 5 mm probe head at the Ruđer Bošković Institute (Zagreb, Croatia). The ^{1}H and ^{13}C NMR spectra were recorded at 600.130 and 150.903 MHz, respectively. The chemical shifts (δ/ppm) of the ^{1}H spectra were referenced to the peak of the residual solvent ($CDCl_3$, ^{1}H: 7.26 ppm), and the chemical shifts of the ^{13}C spectra, to the $CDCl_3$-*d* signal (^{13}C: δ = 77.23 ppm). Unless otherwise indicated, all spectra were recorded at 298 K. The assignment of the ^{1}H and ^{13}C signals in the NMR spectra of the compounds was confirmed by cross peaks in the 2D spectra: ^{1}H−^{1}H COSY (correlation spectroscopy), ^{1}H−^{1}H NOESY (nuclear Overhauser effect spectroscopy), ^{1}H−^{13}C HMQC (heteronuclear multiple quantum coherence), and ^{1}H−^{13}C HMBC (heteronuclear multiple bond correlation). In the case of the $CDCl_3$-*d*/DMSO-d_6 mixture, calibration was performed using TMS as an internal standard. NMR titrations were performed by adding 10 μL portions of DMSO-d_6 to NMR tubes containing $CDCl_3$-*d* solutions of the peptides under study (c = 2.5 × 10^{-2} M). Spectra were recorded after each addition, and DMSO-d_6 was added until no change in the chemical shift of the amide protons was observed. CD spectra were recorded using a Jasco-810 spectropolarimeter in CH_2Cl_2 or KBr. Molar ellipticity coefficients [θ] are given in degrees, concentration c in mol L^{-1}, and path length l in cm, so the unit for [θ] is deg cm^2 dmol^{-1}. Mass spectra were recorded using an HPLC-MS system coupled to a triple-quadrupole mass spectrometer, operating in a positive or negative ESI mode. Samples were dissolved in 100% methanol at a concentration of 1 mg/mL and then diluted in 0.1% formic acid to a final concentration of 1 μg/mL. Samples were analyzed using a high-resolution nanoESI-Q-TOF mass spectrometer (Synapt G2-Si, Waters, Milford, MA, USA) coupled with a liquid chromatograph (nanoACQUITY UPLC, Waters, Milford, MA, USA). Mass spectra were obtained by positive ionization in resolution mode. Data were acquired every second in the mass range from 50 to 800 Da. The mass accuracy of the raw data was corrected by infusing leucine enkephalin (1 ng/μL, 0.4 μL/min flow rate, 556.2771 Da [M + H]$^+$) into the mass spectrometer as a reference mass during sample analysis. Melting points were determined using a Reichert Thermovar apparatus. Single crystal measurements were performed with an Oxford Diffraction Xcalibur Nova R.

*Syntheses of Boc−L−Ala−L−Pro−NH−Fn−COOMe (**4**), Boc−D−Ala−L−Pro−NH−Fn−COOMe (**5**), Boc−L−Ala−D−Pro−NH− Fn−COOMe (**6**), and Boc−D−Ala−D−Pro−NH−Fn−COOMe (**7**).* A suspension of the Boc−NH−Fn−COOMe (**1**)[38] (500 mg, 1.4 mmol) in dry CH_2Cl_2 (5 mL) was purged with HCl_{gas} at 0 °C for 30 min. Then the solvent was evaporated *in vacuo*, and the obtained hydrochloride salt was suspended in CH_2Cl_2 and treated with NEt_3 (pH ≈ 8) to give an unstable free amine suitable for coupling to Boc−L−Pro−OH and Boc−D−Pro−OH (610 mg, 2.8 mmol), respectively, using the standard EDC/HOBt method [EDC (644 mg, 3.36 mmol); HOBt (454 mg, 3.36 mmol)]. The reaction mixtures were stirred at room temperature for ∼1 h until TLC monitoring showed complete consumption of the free amine. The standard workup (washing with a saturated aqueous solution of $NaHCO_3$, a 10% aqueous solution of citric acid and brine, drying over Na_2SO_4, and evaporating *in vacuo*) was followed with TLC purification of the crude products Boc−L−Pro−NH−Fn−COOMe (**2**) (83%) [(CH_2Cl_2:EtOAc = 5:1); R_f = 0.33] and Boc−D−Pro−NH−Fn−COOMe (**3**) (90%) [(CH_2Cl_2:EtOAc = 5:1); R_f = 0.35]. Subsequently, peptides **2** and **3** (800 mg, 1.75 mmol) were deprotected with HCl_{gas} as described above, and the free amines obtained were coupled with Boc−L−Ala−OH and Boc−D−Ala−OH (662 mg, 3.5 mmol), respectively, using the standard EDC/HOBt method [EDC (805 mg, 4.2 mmol); HOBt (567 mg, 4.2 mmol)]. The standard workup was employed to obtain products which were purified by TLC on silica gel [EtOAc; R_f = 0.78 (**4**), R_f = 0.61 (**5**), R_f = 0.66 (**6**), R_f = 0.72 (**7**)] to give orange solids of **4** (800 mg, 87%), **5** (830 mg, 90%), **6** (730 mg, 80%), and **7** (600 mg, 65%). The results of IR and NMR analyses of compounds **4** and **5** are in a good agreement with literature data.[14]

*Boc−D−Pro−NH−Fn−COOMe (**3**).* Mp = 125−128 °C. R_f = 0.33 (CH_2Cl_2:EtOAc = 5:1). IR (CH_2Cl_2) $\bar{\nu}_{max}$/cm^{-1}: 3406 s (NH_{free}), 3284, 3232 m ($NH_{assoc.}$), 1706 s, 1692 s, 1655 s ($C{=}O_{COOMe}$, $C{=}O_{CONH}$), 1560 s, 1532 s, 1476 s, 1467 s (amide II). ^{1}H NMR (600 MHz, $CDCl_3$-*d*): δ 8.54 (br s, 0.66H, NH_{Fn}), 4.81−4.65 (m, 2.60H, H-7$_{Fn}$, H-10$_{Fn}$ and H-2/5$_{Fn}$), 4.62−4.50 (m, 1.23H, H-2/5$_{Fn}$), 4.43−4.30 (m, 2.84H, H-8$_{Fn}$, H-9$_{Fn}$ and CH-α_{Pro}), 4.08−3.96 (m, 1.87H, H-3$_{Fn}$ and H-4$_{Fn}$), 3.80 (s, 3H, CH_{3}-$_{COOMe}$), 3.51−3.40 (m, 1H, CH_2-δ_{Pro}), 3.40−3.30 (m, 0.71H, CH_2-δ'_{Pro}), 2.53−2.36 (m, 0.73H, CH_2-β_{Pro}), 2.03−1.96 (m, 1H, CH_2-γ_{Pro}), 1.96−1.82 (m, 1.75H, CH_2-β'_{Pro} and CH_2-γ'_{Pro}), 1.51 (s, 9H, $(CH_3)_{3}$-$_{Boc}$) ppm. ^{13}C NMR (150 MHz, $CDCl_3$-*d*): δ 171.9 (CO_{COOMe}), 170.3 (CO_{Fca}), 156.6 (CO_{Boc}), 95.9 (C-1$_{Fn}$), 81.0 (C_{qBoc}), 72.9(C-8/9$_{Fn}$), 72.8 (C-8/9$_{Fn}$), 72.0 (C-6$_{Fn}$), 71.4 (C-7/10$_{Fn}$), 71.1 (C-7/10$_{Fn}$), 66.6 (C-3$_{Fn}$ and C-4$_{Fn}$), 63.0 (C-2$_{Fn}$ and C-5$_{Fn}$), 60.4 (CH-α_{Pro}), 51.8 (CH_{3}-$_{COOMe}$), 47.4 (CH_2-δ_{Pro}), 28.6 [$(CH_3)_{3}$-$_{Boc}$], 27.5 (CH_2-β_{Pro}), 24.9 (CH_2-γ_{Pro}) ppm. Anal. Calcd for $C_{22}H_{28}N_2O_5Fe$: 456.1. ESI-MS (H_2O:MeOH = 50:50): [(M − H)$^-$] m/z 455.1, [(M + Na)$^+$] m/z 479.

*Boc−L−Ala−D−Pro−NH−Fn−COOMe (**6**).* Mp = 98 °C. R_f = 0.66 (EtOAc). IR (CH_2Cl_2) $\bar{\nu}_{max}$/cm^{-1}: 3429 s (NH_{free}), 3341, 3303 m ($NH_{assoc.}$), 1707 s, 1670 s, 1621 s ($C{=}O_{COOMe}$, $C{=}O_{CONH}$), 1549 s, 1503 s, 1460 s, 1423 s (amide II). ^{1}H NMR (600 MHz, $CDCl_3$-*d*): δ 8.41 (br s, 1H, NH_{Fn}), 5.52 (d, J = 6.06 Hz, 1H, NH_{Ala}), 4.76−4.73 (m, 1H, H-7/10$_{Fn}$), 4.73−4.70 (m, 1H, H-7/10$_{Fn}$), 4.68−4.61 (m, 3H, H-2$_{Fn}$, H-5$_{Fn}$ and CH-α_{Pro}), 4.51−4.44 (m, 1H, CH-α_{Ala}), 4.39−4.37 (m, 2H, H-8$_{Fn}$ and H-9$_{Fn}$), 4.01−3.99 (m, 2H, H-3$_{Fn}$ and H-4$_{Fn}$),

https://doi.org/10.1021/acs.organomet.4c00248
Organometallics 2024, 43, 2608−2625

3.90−3.85 (m, 1H, CH_2-δ_{Pro}), 3.79 (s, 3H, CH_3-$_{COOMe}$), 3.54−3.48 (m, 1H, CH_2-δ'_{Pro}), 2.51−2.47 (m, 1H, CH_2-β_{Pro}), 2.22−2.13 (m, 1H, CH_2-γ_{Pro}), 2.09−2.01 (m, 1H, CH_2-γ'_{Pro}), 1.96−1.92 (m, 1H, CH_2-β'_{Pro}), 1.39 (s, 9H, $(CH_3)_3$-$_{Boc}$), 1.35 (d, J = 6.89 Hz, 3H, CH_3-$_{Ala}$) ppm. ^{13}C NMR (150 MHz, $CDCl_3$-d): δ 173.2 (CO_{Ala}), 172.1 (CO_{COOMe}), 169.2 (CO_{Fn}), 155.6 (CO_{Boc}), 95.6 (C-1_{Fn}), 80.0 (C_{qBoc}), 72.7 (C-8/9_{Fn}), 72.6 (C-8/9_{Fn}), 71.7 (C-6_{Fn}), 71.35 (C-7/10_{Fn}), 71.34 (C-7/10_{Fn}), 66.4 (C-3/4_{Fn}), 66.1 (C-3/4_{Fn}), 63.3 (C-2/5_{Fn}), 63.1 (C-2/5_{Fn}), 60.9 (CH-α_{Pro}), 51.7 (CH_3-$_{COOMe}$), 48.4 (CH-α_{Ala}), 47.3 (CH_2-δ_{Pro}), 28.5 [$(CH_3)_3$-$_{Boc}$], 27.8 (CH_2-β_{Pro}), 24.9 (CH_2-γ_{Pro}), 17.7 (CH_3-$_{Ala}$) ppm. Anal. Calcd for $C_{25}H_{33}N_3O_6Fe$: 527.4, ESI-MS (H_2O:MeOH = 50:50): [$(M - H)^-$] m/z 526.1, [$(M + H)^+$] m/z 528.1. nanoESI-Q-TOF-HRMS m/z = 528.1797 (calculated for $C_{25}H_{33}FeN_3O_6$ = 528.1797).

*Boc−D−Ala−D−Pro−NH−Fn−COOMe (**7**).* Mp = 180 °C. R_f = 0.72 (EtOAc). IR (CH_2Cl_2) $\overline{\nu}_{max}/cm^{-1}$: 3431 s ($NH_{free}$), 3305, 3240 m ($NH_{assoc.}$), 1706 s, 1695 s, 1637 s (C═O_{COOMe}, C═O_{CONH}), 1558 s, 1544 s, 1539 s (amide II). ^{1}H NMR (600 MHz, $CDCl_3$-d): *trans* isomer: δ 8.46 (br s, 1H, NH_{Fn}), 5.35 (d, J = 7.66 Hz, 1H, NH_{Ala}), 4.77−4.74 (m, 1H, H-7/10_{Fn}), 4.73−4.69 (m, 1H, H-7/10_{Fn}), 4.68−4.62 (s, 2.4H, CH-α_{Pro} and H-2/5_{Fn}), 4.54−4.47 (m, 2H, CH_{Ala} and H-2/5_{Fn}), 4.37−4.35 (m, 1H, H-8/9_{Fn}), 4.35−4.26 (m, 1.6H, H-8/9_{Fn}), 4.01−3.99 (m, 1H, H-3/4_{Fn}), 3.99−3.95 (m, 1.2H, H-3/4_{Fn}), 3.79 (s, 3H, CH_3-$_{COOMe}$), 3.71−3.63 (m, 1H, CH_2-δ_{Pro}), 3.62−3.55 (m, 1.5H, CH_2-δ'_{Pro}), 2.49−2.41 (m, 1H, CH_2-β_{Pro}), 2.22−2.12 (m, 1.2H, CH_2-γ_{Pro}), 2.07−1.97 (m, 1.6H, CH_2-γ'_{Pro}), 1.95−1.86 (m, 1.5H, CH_2-β'_{Pro}), 1.44 (s, 14H, $(CH_3)_3$-$_{Boc}$), 1.38 (d, J = 6.91 Hz, 3H, CH_3-$_{Ala}$) ppm. ^{13}C NMR (150 MHz, $CDCl_3$-d): δ 173.8 (CO_{Ala}), 171.7 (CO_{COOMe}), 169.2 (CO_{Fn}), 155.3 (CO_{Boc}), 95.6 (C-1_{Fn}), 80.0 (C_{qBoc}), 72.7 (C-8/9_{Fn}), 72.6 (C-8/9_{Fn}), 72.1 (C-6_{Fn}), 71.8 (C-7/10_{Fn}), 71.3 (C-7/10_{Fn}), 66.5 (C-3/4_{Fn}), 66.3 (C-3/4_{Fn}), 63.30 (C-2/5_{Fn}), 62.8 (C-2/5_{Fn}), 60.5 (C-α_{Pro}), 51.8 (CH_3-$_{COOMe}$), 48.0 (CH-α_{Ala}), 47.5 (CH_2-δ_{Pro}), 28.5 [$(CH_3)_3$-$_{Boc}$], 26.8 (CH_2-β_{Pro}), 25.3 (CH_2-γ_{Pro}), 18.6 (CH_3-$_{Ala}$) ppm. ^{1}H NMR (600 MHz, $CDCl_3$-d) *cis* isomer: δ 8.83 (s, 0.18H, NH_{Fn}), 5.14 (d, J = 5.90 Hz, 0.24H, NH_{Ala}), 4.93−4.90 (m, 0.21H, H-2/5_{Fn}), 4.89−4.86 (m, 0.20H, H-2/5_{Fn}), 4.67−4.64 (m, 2.37H, H-7_{Fn} and H-10_{Fn}), 4.53−4.47 (m, 2.12H, CH-α_{Ala}), 4.44−4.40 (m, 0.22H, CH-α_{Pro} and H-8/9_{Fn}), 4.35−4.28 (m, 1.63H, H-8/9_{Fn}), 4.07−4.05 (m, 0.21H, H-3/4_{Fn}), 4.00−3.97 (m, 1.22H, H-3/4_{Fn}), 3.76 (s, 0.56H, CH_3-$_{COOMe}$), 3.64−3.58 (m, 1.47H, CH_2-δ_{Pro} and CH_2-δ'_{Pro}), 2.74−2.69 (m, 0.19H, CH_2-β_{Pro}), 2.24−2.14 (m, 1.25H, CH_2-γ_{Pro}), 2.09−2.00 (m, 1.62H, CH_2-γ'_{Pro}), 1.97−1.89 (m, 1.50H, CH_2-β'_{Pro}), 1.51 (s, 1.64H, $(CH_3)_3$-$_{Boc}$), 1.32 (d, J = 6.74 Hz, 0.74H, CH_3-$_{Ala}$) ppm. ^{13}C NMR (150 MHz, $CDCl_3$-d): δ 172.8 (CO_{Ala}), 172.5 (CO_{COOMe}), 168.9 (CO_{Fn}), 156.7 (CO_{Boc}), 96.2 (C-1_{Fn}), 80.6 (C_{qBoc}), 72.5 (C-8/9_{Fn}), 72.4 (C-8/9_{Fn}), 72.0 (C-6_{Fn}), 71.7 (C-7/10_{Fn}), 71.0 (C-7/10_{Fn}), 66.6 (C-3/4_{Fn}), 65.9 (C-3/4_{Fn}), 63.4 (C-2/5_{Fn}), 63.1 (C-2/5_{Fn}), 61.5 (CH-α_{Pro}), 51.8 (CH_3-$_{COOMe}$), 49.1 (CH-α_{Ala}), 46.8 (CH_2-δ_{Pro}), 31.3 (CH_2-β_{Pro}), 28.5 [$(CH_3)_3$-$_{Boc}$], 22.3 (CH_2-γ_{Pro}), 16.6 (CH_3-$_{Ala}$) ppm. Anal. Calcd for $C_{25}H_{33}N_3O_6Fe$: 527.4. ESI-MS (H_2O:MeOH = 50:50): [$(M - H)^-$] na m/z 526.1, [$(M + Na)^+$] na m/z 550. nanoESI-Q-TOF-HRMS m/z = 528.1802 (calculated for $C_{25}H_{33}FeN_3O_6$ = 528.1797).

*Syntheses of Ac−L−Ala−L−Pro−NH−Fn−COOMe (**8**), Ac−D−Ala−L−Pro−NH−Fn−COOMe (**9**), Ac−L−Ala−D−Pro−NH−Fn−COOMe (**10**), and Ac−D−Ala−D−Pro−NH−Fn−COOMe (**11**).* Acetamides **8**−**11** were prepared from carbamates **4**−**7** (800 mg, 1.52 mmol) through the Boc-deprotection in an acidic medium as described above. The hydrochloride salts obtained were treated with NEt_3 (0.99 mL, 7.12 mmol) to give free amines, which were cooled at 0 °C before acetyl chloride (649 μL, 9.12 mmol) was added dropwise and then stirred further in an ice bath. After TLC monitoring showed complete conversion of the starting materials, the reaction mixtures were poured into water and extracted with CH_2Cl_2. The combined organic phases were washed with a brine, dried over Na_2SO_4, and evaporated to dryness *in vacuo*. The resulting crude products were purified by TLC on silica gel [EtOAc; R_f = 0.65 (**8**), R_f = 0.61 (**9**), R_f = 0.60 (**10**), R_f = 0.64 (**11**)] to give orange solids of **8** (851 mg, 56%), **9** (912 mg, 60%), **10** (1.063 g, 70%), and **11** (912 mg, 60%). The results of IR and NMR analyses of compounds **8** and **9** agree well with literature data.[14]

*Ac−L−Ala−D−Pro−NH−Fn−COOMe (**10**).* Mp = 102 °C. R_f = 0.60 (EtOAc). IR (CH_2Cl_2) $\overline{\nu}_{max}/cm^{-1}$: 3438 s ($NH_{free}$), 3322 s ($NH_{assoc.}$), 1708 s, 1670, 1657 (C═O_{COOMe}, C═O_{CONH}), 1546, 1509 (amide II). ^{1}H NMR (600 MHz, $CDCl_3$-d): δ 8.34 (s, 1H, NH_{Fn}), 6.78 (d, J = 5.87 Hz, 1H, NH_{Ala}), 4.77−4.75 (m, 1H, H-2/5_{Fn}), 4.74−4.72 (m, 1H, H-7/10_{Fn}), 4.70−4.68 (m, 1H, H-2/5_{Fn}), 4.68−4.64 (m, 2H, H-7/10_{Fn}, and CH-α_{Pro}), 4.64−4.60 (m, 1H, CH-α_{Ala}), 4.44−4.41 (m, 1H, H-8/9_{Fn}), 4.40−4.38 (m, 1H, H-8/9_{Fn}), 4.03−4.01 (m, 1H, H-3/4_{Fn}), 4.01−3.99 (m, 1H, H-3/4_{Fn}), 3.96−3.90 (m, 1H, CH_2-δ_{Pro}), 3.79 (s, 3H, CH_3-$_{COOMe}$), 3.56−3.50 (m, 1H, CH_2-δ'_{Pro}), 2.44−2.40 (m, 1H, CH_2-β_{Pro}), 2.17−2.10 (m, 1H, CH_2-γ_{Pro}), 2.07−1.95 (m, 2H, CH_2-β'_{Pro} and CH_2-γ'_{Pro}), 2.03 (s, 3H, CH_3-$_{Ac}$), 1.38 (d, J = 6.69 Hz, 3H, CH_3-$_{Ala}$) ppm. ^{13}C NMR (150 MHz, $CDCl_3$-d): δ 172.6 (CO_{Ala}), 172.4 (CO_{COOMe}), 170.8 (CO_{Ac}), 169.3 (CO_{Fn}), 95.9 (C-1_{Fn}), 73.0 (C-8/9_{Fn}), 72.8 (C-8/9_{Fn}), 71.6 (C-6_{Fn}), 71.4 (C-7/10_{Fn}), 71.2 (C-7/10_{Fn}), 66.4 (C-3/4_{Fn}), 66.2 (C-3/4_{Fn}), 63.08 (C-2/5_{Fn}), 63.04 (C-2/5_{Fn}), 61.1 (CH-α_{Pro}), 51.8 (CH_3-$_{COOMe}$), 47.7 (CH-α_{Ala}), 47.4 (CH_2-δ_{Pro}), 28.4 (CH_2-β_{Pro}), 24.7 (CH_2-γ_{Pro}), 23.0 (CH_3-$_{Ac}$), 16.9 (CH_3-$_{Ala}$) ppm. Anal. Calcd for $C_{22}H_{27}N_3O_5Fe$: 469.3. ESI-MS (H_2O:MeOH= 50:50): [$(M - H)^-$] m/z 468.1, [$(M + Na)^+$] m/z 492. nanoESI-Q-TOF-HRMS m/z = 470.1384 (calculated for $C_{22}H_{27}FeN_3O_5$ = 470.1378).

*Ac−D−Ala−D−Pro−NH−Fn−COOMe (**11**).* Mp = 60 °C. R_f = 0.64 (EtOAc). IR (CH_2Cl_2) $\overline{\nu}_{max}/cm^{-1}$: 3421 s ($NH_{free}$), 3292 s ($NH_{assoc.}$), 1706 s, 1671, 1636 (C═O_{COOMe}, C═O_{CONH}), 1555, 1538, 1508 (amide II). ^{1}H NMR (600 MHz, $CDCl_3$-d) *trans* isomer: δ 8.46 (s, 1H, NH_{Fn}), 6.53 (d, J = 7.3 Hz, 1H, NH_{Ala}), 4.82−4.76 (m, 1H, CH-α_{Ala}), 4.77−4.75 (m, 1H, H-7/10_{Fn}), 4.73−4.70 (m, 1H, H-7/10_{Fn}), 4.70−4.67 (m, 1H, H-2/5_{Fn}), 4.61 (dd, J = 7.8; 2.2 Hz, 1.2H, CH-α_{Pro}), 4.49−4.46 (m, 1H, H-2/5_{Fn}), 4.39−4.37 (m, 1H, H-8/9_{Fn}), 4.37−4.34 (m, 1H, H-8/9_{Fn}), 4.01−3.98 (m, 2H, H-3/4_{Fn}), 3.79 (s, 3H, CH_3-$_{COOMe}$), 3.76−3.70 (m, 1H, CH_2-δ_{Pro}), 3.65−3.61 (m, 1H, CH_2-δ'_{Pro}), 2.46−2.40 (m, 1H, CH_2-β_{Pro}), 2.26−2.16 (m, 1H, CH_2-γ_{Pro}), 2.09−2.03 (m, 1H, CH_2-γ'_{Pro}), 2.00 (s, 3H, CH_3-$_{Ac}$), 2.00−1.92 (m, 1H, CH_2-β'_{Pro}), 1.41 (d, J = 6.8 Hz, 3H, CH_3-$_{Ala}$) ppm. ^{13}C NMR (150 MHz, $CDCl_3$-d): δ 173.3 (CO_{Ala}), 171.8 (CO_{COOMe}), 169.7 (CO_{Fn}), 169.2 (CO_{Ac}), 95.6 (C-1_{Fn}), 72.7 (C-8/9_{Fn}), 72.5 (C-8/9_{Fn}), 72.1 (C-6_{Fn}), 71.4 (C-7/10_{Fn}), 71.1 (C-7/10_{Fn}), 66.43 (C-3/4_{Fn}), 66.39 (C-3/4_{Fn}), 63.1 (C-2/5_{Fn}), 62.8 (C-2/5_{Fn}), 60.6 (CH-α_{Pro}), 51.8 (CH_3-$_{COOMe}$), 47.6 (CH_2-δ_{Pro}), 46.8 (CH-α_{Ala}), 27.3 (CH_2-β_{Pro}), 25.3 (CH_2-γ_{Pro}), 23.3 (CH_3-$_{Ac}$), 18.4 (CH_3-$_{Ala}$) ppm. ^{1}H NMR (600 MHz, $CDCl_3$-d) *cis* isomer: δ 9.13 (s, 0.16H, NH_{Fca}), 6.30 (d, J = 4.7 Hz, 0.16H, NH_{Ala}), 4.97−4.94 (m, 0.15H, H-2/5_{Fn}), 4.89−4.86 (m, 0.17H, H-2/5_{Fn}), 4.73−4.70 (m, 1.18H, H-7/10_{Fn}), 4.65−4.61 (m, 1.16H, H-7/10_{Fn}), 4.45−4.40 (m, 0.36H, CH-α_{Pro} and CH-α_{Ala}), 4.37−4.34 (m, 1.13H, H-8/9_{Fn}), 4.34−4.33 (m, 0.17H, H-8/9_{Fn}), 4.06−4.04 (m, 0.18H, H-3/4_{Fn}), 4.02−3.98 (m, 2.16H, H-3/4_{Fn}), 3.78 (s, 0.50H, CH_3-$_{COOMe}$), 3.69−3.61 (m, 1.40H, CH_2-δ_{Pro} and CH_2-δ'_{Pro}), 2.72−2.67 (m, 0.18H, CH_2-β_{Pro}), 2.26−2.17 (m, 1.18H, CH_2-γ_{Pro}), 2.09−2.03 (m, 2.05H, CH_2-γ'_{Pro}), 2.05 (s, 2.05H, CH_3-$_{Ac}$), 2.00−1.92 (m, 1.58H, CH_2-β'_{Pro}), 1.36 (d, J = 6.9 Hz, 0.68H, CH_3-$_{Ala}$) ppm. ^{13}C NMR (150 MHz, $CDCl_3$-d): δ 172.0 (CO_{Ala}), 171.9 (CO_{COOMe}), 171.2 (CO_{Fn}), 168.8 (CO_{Ac}), 96.2 (C-1_{Fn}), 72.6 (C-8/9_{Fn}), 72.4 (C-8/9_{Fn}), 71.9 (C-6_{Fn}), 71.4 (C-7/10_{Fn}), 71.0 (C-7/10_{Fn}), 66.6 (C-3/4_{Fn}), 66.0 (C-3/4_{Fn}), 63.5 (C-2/5_{Fn}), 63.2 (C-2/5_{Fn}), 61.5 (CH-α_{Pro}), 51.7 (CH_3-$_{COOMe}$), 46.7 (CH-α_{Ala}), 47.6 (CH_2-δ_{Pro}), 31.4 (CH_2-β_{Pro}), 22.8 (CH_2-γ_{Pro}), 22.8 (CH_3-$_{Ac}$), 16.4 (CH_3-$_{Ala}$) ppm. Anal. Calcd for $C_{22}H_{27}N_3O_5Fe$: 469.3 ESI-MS (H_2O:MeOH= 50:50): [$(M - H)^-$] m/z 468.1, [$(M + H)^{-+}$] m/z 492. nanoESI-Q-TOF-HRMS m/z = 470.1383 (calculated for $C_{22}H_{27}FeN_3O_5$ = 470.1378).

Computational Details. Conformational analyses of Boc-protected **6** and **7** and Ac-protected **10** and **11** were conducted in three stages. The same scalar properties were expected for their enantiomeric pairs, thus they were not individually modeled. In the first stage, a series of low-level optimizations were performed by molecular mechanics (OPLS2005 force field) in MacroModel.[105,106] Only the representative set of the most stable conformers was selected for further

https://doi.org/10.1021/acs.organomet.4c00248
Organometallics 2024, 43, 2608−2625

Table 3. Crystallographic, Data Collection, and Refinement Data

Compound	4	3
empirical formula	$C_{25}H_{33}FeN_3O_6$	$C_{22}H_{28}FeN_2O_5$
formula wt/g mol^{-1}	527.39	456.31
crystal dimensions/mm	0.25 × 0.23 × 0.11	0.23 × 0.18 × 0.12
space group	$P\,4_1\,2_1\,2$	$P\,2_1$
a/Å	11.06960(10)	10.94960(10)
b/Å	11.06960(10)	8.57190(10)
c/Å	43.0202(5)	11.94590(10)
α/deg	90	90
β/deg	90	107.3410(10)
γ/deg	90	90
Z	8	2
V/Å^3	5271.53(11)	1070.266(19)
D_{calc}/g cm^{-3}	1.329	1.416
μ/mm^{-1}	4.949	5.954
Θ range/deg	4.11−79.77	3.88−79.76
T/K	293(2)	293(2)
radiation wavelength/Å	1.54184	1.54184
diffractometer type	Synergy S	Synergy S
ranges of h, k, l	$-13 < h < 13$:	$-13 < h < 13$;
	$-10 < k < 13$;	$-10 < k < 10$;
	$-54 < l < 54$	$-12 < l < 15$
reflections collected	40483	15128
independent reflections	5683	4544
observed reflections ($I \geq 2\sigma$)	5166	4354
absorption correction	multiscan	multiscan
T_{min}, T_{max}	0.4113, 1.0000	0.5397, 1.0000
R_{int}	0.0782	0.0601
$R(F)$	0.0346	0.0405
$R_w(F^2)$	0.0979	0.1158
goodness of fit	1.073	0.844
Flack parameter	−0.012(3)	−0.006(4)
H atom treatment	constrained	constrained
no. of parameters	316	271
no. of restraints	0	0
$\Delta\rho_{max}$, $\Delta_{\rho min}$, $\Delta\rho_{rms}$ (e Å^{-3})	0.222, −0.230, 0.036	0.357, −0.423, 0.065

optimizations at a high level of theory (B3LYP/Lanl2DZ) and run in Gaussian 16 with a default grid and convergence criteria.[107] The last stage included optimizations of the most stable conformers at the B3LYP/6-311+G(d,p) (LanL2DZ basis set on Fe) level of theory while surrounding solvent (chloroform) was described as a polarizable continuum (PCM).[108] Each structure was verified as a minimum on the potential energy surface. The reported energies refer to standard Gibbs free energies at 298 K. QTAIM theory implemented in the AIMAll package[109] was used for the characterization of hydrogen bonds. Topological parameters of the bond critical points between the hydrogen bond acceptors and hydrogen atoms were calculated and N−H···O verified according to the Koch and Popelier criteria.[110]

Crystallographic Study. Single crystal measurements were performed on a dual source (Mo/Cu) Rigaku Oxford Diffraction Synergy S diffractometer equipped with an Oxford Cryosystems series 800 cryostat. Friedel pairs were measured to establish the absolute configuration of stereogenic centers. Program package CrysAlis PRO[111] was used for data reduction and multiscan absorption correction. The structures were solved using SHELXS97[112] and refined with SHELXL-2017.[113] Absolute configurations were determined from an anomalous dispersion. Models were refined using the full-matrix least-squares refinement; all non-hydrogen atoms were refined anisotropically. Hydrogen atoms were located in a difference Fourier map and refined as riding entities. Molecular geometry calculations were performed with PLATON,[114] and molecular graphics were prepared using ORTEP-3[115] and Mercury.[116] Crystallographic and refinement data for the structures reported in this article are shown in Table 3.

Biological Evaluation. *Antimicrobial Activity.* Antimicrobial activity was tested using the disk diffusion method according to the protocol described in detail in our recent work.[16] Briefly, Gram-positive bacteria (*Staphylococcus aureus*, *Bacillus subtilis*, *Enterococcus faecium*, and *Listeria monocytogenes*), Gram-negative bacteria (*Pseudomonas aeruginosa*, *Escherichia coli*, and *Salmonella enterica s. Typhimurium*), lactic acid bacteria (*Leuconostoc mesenteroides*and *Lactobacillus plantarum*) and yeasts (*Candida albicans*, *Candida utiliz*, *Rhodotorula sp*, and *Saccharomyces cerevisiae*) were used to evaluate the antimicrobial properties of the tested peptides. In addition, Boc-peptides **4**−**7** were tested at a concentration of 188.89 mM, while Ac-peptides **8**−**11** were tested at a concentration of 213.16 mM. It can be calculated that the compounds were tested at a level of 1 mg/disk.

In addition, the efficacy of the antimicrobial activity was tested by exposing the cells to the tested peptides dissolved in DMSO or the peptide-cyclodextrin inclusion complex. To prepare the peptide-cyclodextrin inclusion complex, an aqueous solution of methyl-β-cyclodextrin (MBCD) (Sigma-Aldrich, USA) was prepared at a concentration of 20 mM. Equal volumes of 20 mM peptide compounds **4**−**7** and MBCD were mixed and stirred on a vortex shaker at room temperature for 2 h. Then the prepared compounds were incubated for 24 h with a cell suspension in buffer (6 log CFU, peptide concentrations 4 and 2 mM). After 4, 8, and 24 h of incubation, decimal dilutions were prepared and plated on agar. As a control, cells without peptide exposure were also plated on agar. The

https://doi.org/10.1021/acs.organomet.4c00248
Organometallics 2024, 43, 2608−2625

following day, the colonies on the plates were counted and the survival rate was calculated for the control and the cells exposed to the tested tripeptide dissolved in DMSO or the peptide-cyclodextrin inclusion complex. The survival rate was calculated by dividing the total number of cells surviving after 4, 8, and 24 h of incubation (log CFU) by the total number (log CFU) of living cells before treatment.

Antiradical Activity. *DPPH Assay.* The antiradical activity of ferrocene compounds (concentration of 1 mM) against DPPH (1,1-diphenyl-2-picrylhydrazyl) radicals was measured according to the method of Brand-Williams et al.[117] Samples (60 μL) were mixed with 0.1 mM DPPH working solution (2 mL). Absorbance at 517 nm was measured with a spectrophotometer after 30 min of incubation in the dark. Ethanol was used as a control. A calibration curve was constructed using Trolox as the reference antioxidant in the range of 0.05−0.5 mM (R^2 = 0.997). Results were expressed as millimoles of Trolox equivalents (mM Trolox equivalents). Measurements were performed in triplicate.

ABTS Radical Cation Scavenging Activity. The ABTS radical scavenging activity of the tested compounds was estimated according to the method of Re et al.[118] ABTS·+ was generated in the reaction of a 7 mM stock solution of ABTS [2,2′-azinobis(3-ethylbenzothiazoline-6-sulfonic acid) diammonium salt] with 140 mM potassium persulfate, and the mixture was left in the dark at room temperature for 16 h before use. Then, the ABTS·+ working solution was prepared by diluting the previously prepared mixture with 96% (v/v) ethanol until an initial absorbance value of 0.70 ± 0.02 at 734 nm was obtained. Briefly, 20 μL of sample was added to 2 mL of ABTS·+ working solution, and the absorbance at 734 nm was measured after 6 min. Trolox (0.1−1.5 mM) was used as a reference antioxidant (R^2 = 0.999). A control was prepared with the same volume of ethanol without test compounds or reference antioxidant. The ABTS·+ scavenging activity of the samples was expressed in millimoles of Trolox (mM Trolox). Measurements were performed in triplicate.

Antiproliferative Activity. The antiproliferative activity was evaluated in vitro using the CellTiter 96 AQueous One Solution Cell Proliferation assay (Promega, USA), abbreviated as MTS, as we have previously described.[15] The human tumor adherent cell line HeLa was used, and it was cultivated in DMEM (Sigma-Aldrich, USA) supplemented with 5% (v/v) FBS (GibcoTM, Thermo Fisher Scientific, USA) and 1% (v/v) antibiotic/antimitotic solution (Gibco, Thermo Fisher Scientific, USA). The HeLa cell line was cultured in BioLite Petri dishes (Thermo Fisher Scientific, USA) in an incubator with a humidified atmosphere and 5% CO_2 at 37 °C, while individual tests were performed in 96-well plates (Thermo Fisher Scientific, USA). Briefly, cells were seeded at an initial concentration of 3×10^4 cells per well in 100 μL of culture media and treated after 24 h with the different concentrations of the compounds tested (50, 100, 175, 250, 375, and 500 μM). The treatment lasted for 72 h in the incubator and then was followed by the MTS assay. The assay was carried out according to the manufacturer's instructions with a few modifications. MTS reagent (10 μL) was added to each well, cells were incubated for an additional 3 h, and then the absorbance was measured at 492 nm on the microplate reader (Tecan, Switzerland). The cell viability percentage was expressed as the ratio between the absorbance of the treated versus not treated control cells. The tests were performed in triplicate with four parallels for each concentration. From the cell viability data, when possible, the IC50 value, defined as the concentration of the test compound that results in 50% inhibition of cell growth, was calculated from the best-fit equations of the dose−response curves.

Cell Death Assessment. Quantitative analysis of peptide-treated live, apoptotic, and dead cells was performed using the Muse Cell Analyzer (EMD Millipore Corporation, Burlington, MA, USA) and the Muse Annexin V and Dead Cell Kit according to the manufacturer's instructions. In brief, HeLa cells were plated in a 6-well culture plate at a density of 5 × 104 cells mL^{-1} (2 mL per well) and treated with 250 μM of conjugates **4**, **5**, **8**, and **10** for 72 h. After treatment, both floating and adherent cells were collected, centrifuged at 600*g*, and resuspended in cell culture medium at the appropriate concentration according to the manufacturer's protocol. Then 100 μL aliquots of the cell suspension were mixed with 100 μL of Muse Annexin V and Dead Cell Reagent and incubated for 20 min at room temperature in the dark. The cells were then analyzed using the Muse Cell Analyzer. Each compound was tested in duplicate, and each experiment was repeated twice.

■ ASSOCIATED CONTENT

Supporting Information

The Supporting Information is available free of charge at https://pubs.acs.org/doi/10.1021/acs.organomet.4c00248.

HRMS and ESI-MS data; ^{1}H NMR and ^{13}C NMR spectra; ^{1}H−^{1}H NOESY, ^{1}H−^{1}H COSY, and ^{1}H−^{13}C HMBC spectra; concentration- and temperature-dependent IR spectra; temperature- and solvent-dependent ^{1}H NMR spectra; concentration-dependent NH chemical shifts; the NOE contacts; and DFT data (PDF)

Accession Codes

CCDC 2263034−2263035 contain the supplementary crystallographic data for this paper. These data can be obtained free of charge via www.ccdc.cam.ac.uk/data_request/cif, or by emailing data_request@ccdc.cam.ac.uk, or by contacting The Cambridge Crystallographic Data Centre, 12 Union Road, Cambridge CB2 1EZ, UK; fax: +44 1223 336033.

■ AUTHOR INFORMATION

Corresponding Authors

Ivan Kodrin − *Department of Organic Chemistry, University of Zagreb Faculty of Science, 10000 Zagreb, Croatia;* orcid.org/0000-0001-6353-3187; Email: ikodrin@chem.pmf.hr

Lidija Barišić − *Department of Chemistry and Biochemistry, University of Zagreb Faculty of Food Technology and Biotechnology, 10000 Zagreb, Croatia;* orcid.org/0000-0002-4310-4198; Email: lidija.barisic@pbf.hr

Authors

Monika Kovačević − *Department of Chemistry and Biochemistry, University of Zagreb Faculty of Food Technology and Biotechnology, 10000 Zagreb, Croatia*

Mojca Čakić Semenčić − *Department of Chemistry and Biochemistry, University of Zagreb Faculty of Food Technology and Biotechnology, 10000 Zagreb, Croatia;* orcid.org/0000-0003-3975-1584

Martina Bagović − *Department of Biochemical Engineering, University of Zagreb Faculty of Food Technology and Biotechnology, 10000 Zagreb, Croatia*

Kristina Radošević − *Department of Biochemical Engineering, University of Zagreb Faculty of Food Technology and Biotechnology, 10000 Zagreb, Croatia;* orcid.org/0000-0001-5156-1893

Karla Hanousek Čiča − *Department of Food Engineering, University of Zagreb Faculty of Food Technology and Biotechnology, 10000 Zagreb, Croatia;* orcid.org/0000-0002-5020-0639

Jasna Mrvčić − *Department of Food Engineering, University of Zagreb Faculty of Food Technology and Biotechnology, 10000 Zagreb, Croatia*

Krešimir Molčanov − *Division of Physical Chemistry, Ruđer Bošković Institute, 10000 Zagreb, Croatia*

Sunčica Roca − *NMR Centre, Ruđer Bošković Institute, 10000 Zagreb, Croatia*

Complete contact information is available at:

https://pubs.acs.org/10.1021/acs.organomet.4c00248

Notes

The authors declare no competing financial interest.

■ ACKNOWLEDGMENTS

This work has been fully supported by the Croatian Science Foundation under project IP-2020-02-9162.

■ REFERENCES

(1) Wang, X.; Ni, D.; Liu, Y.; Lu, S. Rational Design of Peptide-Based Inhibitors Disrupting Protein-Protein Interactions. *Front. Chem.* **2021**, *9*, No. 682675.
(2) Seychell, B. C.; Beck, T. Molecular basis for protein-protein interactions. Beilstein J. *Org. Chem.* **2021**, *17*, 1−10.
(3) Lu, H.; Zhou, Q.; He, J.; Jiang, Z.; Peng, C.; Tong, R.; Shi, J. Recent advances in the development of protein-protein interactions modulators: mechanisms and clinical trials. *Signal Transduct. Target Ther.* **2020**, *5*, 213−235.
(4) Hoang, H. N.; Hill, T. A.; Ruiz-Gómez, G.; Diness, F.; Mason, J. M.; Wu, C.; Abbenante, G.; Shepherd, N. E.; Fairlie, D. P. Twists or turns: stabilising alpha vs. beta turns in tetrapeptides. *Chem. Sci.* **2019**, *10*, 10595−10600.
(5) Ovek, D.; Abali, Z.; Zeylan, M. E.; Keskin, O.; Gursoy, A.; Tuncbag, N. Artificial intelligence based methods for hot spot prediction. *Curr. Opin. Struct. Biol.* **2022**, *72*, 209−218.
(6) Laxio Arenas, J.; Kaffy, J.; Ongeri, S. Peptides and peptidomimetics as inhibitors of protein-protein interactions involving *β*-sheet secondary structures. *Curr. Opin. Chem. Biol.* **2019**, *52*, 157−167.
(7) Nair, R. V.; Baravkar, S. B.; Ingole, T. S.; Sanjayan, G. J. Synthetic turn mimetics and hairpin nucleators. *Chem. Commun.* **2014**, *50*, 13874−13884.
(8) Lenci, E.; Trabocchi, A. Peptidomimetic toolbox for drug discovery. *Chem. Soc. Rev.* **2020**, *49*, 3262−3277.
(9) Barišić, L.; Dropučić, M.; Rapić, V.; Pritzkow, H.; Kirin, S. I.; Metzler-Nolte, N. The first oligopeptide derivative of 1′-amino-ferrocene-1-carboxylic acid shows helical chirality with antiparallel strands. *Chem. Commun.* **2004**, *17*, 2004−2005.
(10) Barišić, L.; Čakić Semenčić, M.; Mahmoud, K. A.; Liu, Y.-N.; Kraatz, H.-B.; Pritzkow, H.; Kirin, S. I.; Metzler-Nolte, N.; Rapić, V. Helically Chiral Ferrocene Peptides Containing 1′-Aminoferrocene-1-Carboxylic Acid Subunits as Turn Inducers. *Chem.—Eur. J.* **2006**, *12*, 4965−4980.
(11) Čakić Semenčić, M.; Siebler, D.; Heinze, K.; Rapic, V. Bis- and Trisamides Derived From 1′-Aminoferrocene-1-carboxylic Acid and *α*-Amino Acids: Synthesis and Conformational Analysis. *Organometallics* **2009**, *28*, 2028−2037.
(12) Čakić Semenčić, M.; Heinze, K.; Forster, C.; Rapic, V. Bioconjugates of 1′-Aminoferrocene-1-carboxylic Acid with (S)-3-Amino-2-methylpropanoic Acid and L-Alanine. *Eur. J. Inorg. Chem.* **2010**, *2010*, 1089−1097.
(13) Čakić Semenčić, M.; Barišić, L. Ferrocene Bioconjugates. *Croat. Chem. Acta* **2017**, *90*, 537−569.
(14) Kovačević, M.; Kodrin, I.; Roca, S.; Molčanov, K.; Shen, Y.; Adhikari, B.; Kraatz, H.-B.; Barišić, L. Helically Chiral Peptides That Contain Ferrocene-1,1′-diamine Scaffolds as a Turn Inducer. *Chem.—Eur. J.* **2017**, *23*, 10372−10395.
(15) Kovačević, M.; Čakić Semenčić, M.; Radošević, K.; Molčanov, K.; Roca, S.; Šimunović, L.; Kodrin, I.; Barišić, L. Conformational Preferences and Antiproliferative Activity of Peptidomimetics Containing Methyl 1′-Aminoferrocene-1-carboxylate and Turn-Forming Homo- and Heterochiral Pro-Ala Motifs. *Int. J. Mol. Sci.* **2021**, *22*, 13532−12559.
(16) Kovačević, M.; Markulin, D.; Zelenika, M.; Marjanović, M.; Lovrić, M.; Polančec, D.; Ivančić, M.; Mrvčić, J.; Molčanov, K.; Milašinović, V.; Roca, S.; Kodrin, I.; Barišić, L. Hydrogen Bonding Drives Helical Chirality via 10-Membered Rings in Dipeptide Conjugates of Ferrocene-1,1′-Diamine. *Int. J. Mol. Sci.* **2022**, *23*, 12233−12264.
(17) Moriuchi, T.; Ohmura, S. D.; Moriuchi-Kawakami, T. Chirality Induction in Bioorganometallic Conjugates. *Inorganics* **2018**, *6*, 111−124.
(18) Barišić, L.; Kovačević, M.; Mamić, M.; Kodrin, I.; Mihalić, Z.; Rapić, V. Synthesis and Conformational Analysis of Methyl N-Alanyl-1-aminoferrocene-1-carboxylate. *Eur. J. Inorg. Chem.* **2012**, *2012*, 1810−1822.
(19) Kovačević, M.; Molčanov, K.; Radošević, K.; Srček Gaurina, V.; Roca, S.; Čače, A.; Barišić, L. Conjugates of 1′-aminoferrocene-1-carboxylic acid and proline: synthesis, conformational analysis and biological evaluation. *Molecules* **2014**, *19*, 12852−12880.
(20) Krause, E.; Bienert, M.; Schmieder, P.; Wenschuh, H. The Helix-Destabilizing Propensity Scale of d-Amino Acids: The Influence of Side Chain Steric. *Effects. J. Am. Chem. Soc.* **2000**, *122*, 4865−4870.
(21) Sidorova, A.; Bystrov, V.; Lutsenko, A.; Shpigun, D.; Belova, E.; Likhachev, I. Quantitative Assessment of Chirality of Protein Secondary Structures and Phenylalanine Peptide Nanotubes. *Nanomaterials (Basel)* **2021**, *11*, 3299−3328.
(22) Nuskol, M.; Studen, B.; Meden, A.; Kodrin, I.; Čakić Semenčić, M. Tight turn in dipeptide bridged ferrocenes: Synthesis, X-ray structural, theoretical and spectroscopic studies. *Polyhedron* **2019**, *161*, 137−144.
(23) Nuskol, M.; Šutalo, P.; Djakovic, M.; Kovačević, M.; Kodrin, I.; Čakić Semenčić, M. Testing the Potential of the Ferrocene Chromophore as a Circular Dichroism Probe for the Assignment of the Screw-Sense Preference of Tripeptides. *Organometallics* **2021**, *40*, 1351−1362.
(24) Ganguly, H. K.; Basu, G. Conformational landscape of substituted prolines. *Biophys. Rev.* **2020**, *12*, 25−39.
(25) Byun, B. J.; Song, I. K.; Chung, Y. J.; Ryu, K. H.; Kang, Y. K. Conformational preferences of X-Pro sequences: Ala-Pro and Aib-Pro. *motifs. J. Phys. Chem. B* **2010**, *114*, 14077−14086.
(26) Martin, V.; Legrand, B.; Vezenkov, L. L.; Berthet, M.; Subra, G.; Calmès, M.; Bantignies, J.-L.; Martinez, J.; Amblard, M. Turning Peptide Sequences into Ribbon Foldamers by a Straightforward Multicyclization Reaction. *Angew. Chem., Int. Ed.* **2015**, *54*, 13966−13970.
(27) Metrano, A. J.; Abascal, N. C.; Mercado, B. Q.; Paulson, E. K.; Hurtley, A. E.; Miller, S. J. Diversity of Secondary Structure in Catalytic Peptides with *β*-Turn-Biased Sequences. *J. Am. Chem. Soc.* **2017**, *139*, 492−516.
(28) Singh, A.; Lumb, I.; Mehra, V.; Kumar, V. Correction: Ferrocene-appended pharmacophores: an exciting approach for modulating the biological potential of organic scaffolds. *Dalton Trans.* **2019**, *48*, 2840−2860.
(29) Sharma, B.; Kumar, V. Has Ferrocene Really Delivered Its Role in Accentuating the Bioactivity of Organic Scaffolds? *J. Med. Chem.* **2021**, *64*, 16865−16921.
(30) Ludwig, B. S.; Correia, J. D. G.; Kühn, F. E. Ferrocene derivatives as anti-infective agents. *Coord. Chem. Rev.* **2019**, *396*, 22−48.
(31) Fiorina, V. J.; Dubois, R. J.; Brynes, S. Ferrocenyl polyamines as agents for the chemoimmunotherapy of cancer. *J. Med. Chem.* **1978**, *21*, 393−395.
(32) Astruc, D. Why is Ferrocene so Exceptional? *Eur. J. Inorg. Chem.* **2017**, *2017*, 6−29.
(33) Patra, M.; Gasser, G. The medicinal chemistry of ferrocene and its derivatives. *Nat. Rev. Chem.* **2017**, *1*, 0066.
(34) Jaouen, G.; Vessières, A.; Top, S. Ferrocifen Type Anti Cancer Drugs. *Chem. Soc. Rev.* **2015**, *44*, 8802−8817.
(35) Wang, R.; Chen, H.; Yan, W.; Zheng, M.; Zhang, T.; Zhang, Y. Ferrocene-containing hybrids as potential anticancer agents: Current developments, mechanisms of action and structure-activity relationships. *Eur. J. Med. Chem.* **2020**, *190*, 112109−112129.
(36) Albada, B.; Metzler-Nolte, N. Highly Potent Antibacterial Organometallic Peptide Conjugates. *Acc. Chem. Res.* **2017**, *50*, 2510−2518.

(37) Soulere, L.; Bernard, J. Design, solid phase synthesis and evaluation of cationic ferrocenoyl peptide bioconjugates as potential antioxidant enzyme mimics. *Bioorg. Med. Chem. Lett.* **2009**, *19*, 1173−1176.
(38) Meng, X.; Li, S.; Ma, W.; Wang, J.; Hu, Z.; Cao, D. Synthesis and Antioxidant Activities of Ferrocenyl-containing Curcumin Analogues. *Lett. Drug Des. Discovery* **2018**, *15*, 1252−1258.
(39) Barišić, L.; Rapić, V.; Kovač, V. Ferrocene Compounds. XXIX. Efficient Syntheses of 1′-Aminoferrocene-1-carboxylic Acid Derivatives. *Croat. Chem. Acta.* **2002**, *75*, 199−210.
(40) Mislow, K. Fuzzy restrictions and inherent uncertainties in chirality studies. In *Fuzzy Logic in Chemistry*; Rouvray, D.H., Eds.; Academic Press: New York, 1997; pp 65−90.
(41) Natarajan, R.; Basak, S. C.; Neumann, T. S. Novel approach for the numerical characterization of molecular chirality. *J. Chem. Inf. Model.* **2007**, *47*, 771−775.
(42) Arnaboldi, S.; Benincori, T.; Cirilli, R.; Kutner, W.; Magni, M.; Mussini, P. R.; Noworyta, K.; Sannicolò, F. Inherently chiral electrodes: the tool for chiral voltammetry. *Chem. Sci.* **2015**, *6*, 1706−1711.
(43) Čakić Semenčić, M.; Kodrin, I.; Molčanov, K.; Kovačević, M.; Rapić, V. Novel ferrocene imide derivatives: synthesis, conformational analysis and X-ray structure. *Heliyon* **2022**, *8*, No. e09470.
(44) Kovač, V.; Kodrin, I.; Barišić, L.; Rapić, V. Synthesis and Conformational Study of Bioconjugates Derived from 1-Acetyl-1′-aminoferrocene and α-Amino Acids. *Eur. J. Inorg. Chem.* **2015**, *2015*, 112−123.
(45) Djaković, S.; Kodrin, I.; Smrečki, V.; Novak, P.; Mihalić, Z.; Žiher, D.; Lapić, J.; Rapić, V. 1′-Acetylferrocene Amino Acid Esters and Amides. A simple model for parallel beta-helical peptides. *Tetrahedron* **2014**, *70*, 2330−2342.
(46) Kovač, V.; Čakić Semenčić, M.; Kodrin, I.; Roca, S.; Rapić, V. Ferrocene-dipeptide conjugates derived from aminoferrocene and 1-acetyl-1′-aminoferrocene: synthesis and conformational studies. *Tetrahedron* **2013**, *69*, 10497−10506.
(47) Lapić, J.; Djaković, S.; Kodrin, I.; Mihalić, Z.; Cetina, M.; Rapić, V. Preparation and Conformational Analysis of N-(Ferrocenoyl)-dipeptide Esters and Their 1′-Acetyl Derivatives. *Eur. J. Org. Chem.* **2010**, *2010*, 2512−2524.
(48) Nuskol, M.; Šutalo, P.; Kodrin, I.; Čakić Semenčić, M. Sensing of the Induced Helical Chirality by the Chiroptical Response of the Ferrocene Chromophore. *Eur. J. Inorg. Chem.* **2022**, *2022*, No. e202100880.
(49) Čakić Semenčić, M.; Kodrin, I.; Barišić, L.; Nuskol, M.; Meden, A. Synthesis and Conformational Study of Monosubstituted Aminoferrocene-Based Peptides Bearing Homo- and Heterochiral Pro-Ala Sequences. *Eur. J. Inorg. Chem.* **2017**, *2017*, 306−317.
(50) Kovač, V.; Kodrin, I.; Radošević, K.; Molčanov, K.; Adhikari, B.; Kraatz, H.-B.; Barišić, L. Oxalamide-Bridged Ferrocenes: Conformational and Gelation Properties and In Vitro Antitumor Activity. *Organometallics* **2022**, *41*, 920−936.
(51) Kovačević, M.; Čakić Semenčić, M.; Kodrin, I.; Roca, S.; Perica, J.; Mrvčić, J.; Stanzer, D.; Molčanov, K.; Milašinović, V.; Brkljačić, L.; Barišić, L. Biological Evaluation and Conformational Preferences of Ferrocene Dipeptides with Hydrophobic Amino Acids. *Inorganics* **2023**, *11*, 29.
(52) Vass, E.; Hollósi, M.; Besson, F.; Buchet, R. Vibrational spectroscopic detection of beta- and gamma-turns in synthetic and natural peptides and proteins. *Chem. Rev.* **2003**, *103*, 1917−1954.
(53) Ramos, S.; Thielges, M. C. Site-Specific 1D and 2D IR Spectroscopy to Characterize the Conformations and Dynamics of Protein Molecular Recognition. *J. Phys. Chem. B* **2019**, *123*, 3551−3566.
(54) Jagesar, D. C.; Hartl, F.; Buma, W. J.; Brouwer, A. M. Infrared study of intercomponent interactions in a switchable hydrogen-bonded rotaxane. *Chemistry* **2008**, *14*, 1935−1946.
(55) Joseph, J.; Jemmis, E. D. Red-, Blue-, or No-Shift in Hydrogen Bonds: A Unified Explanation. *J. Am. Chem. Soc.* **2007**, *129*, 4620−4632.
(56) Arunan, E.; Desiraju, G. R.; Klein, R. A.; Sadlej, J.; Scheiner, S.; Alkorta, I.; Clary, D. C.; Crabtree, R. H.; Dannenberg, J. J.; Hobza, P.; Kjaergaard, H. G.; Legon, A. C.; Mennucci, B.; Nesbitt, D. J. Defining the hydrogen bond: An account (IUPAC Technical Report). *Pure Appl. Chem.* **2011**, *83*, 1619−1636.
(57) Fornaro, T.; Burini, D.; Biczysko, M.; Barone, V. Hydrogen-bonding effects on infrared spectra from anharmonic computations: uracil-water complexes and uracil dimers. *J. Phys. Chem. A* **2015**, *119*, 4224−4236.
(58) Ganesh, S.; Jayakumar, R. Role of N-t-Boc group in helix initiation in a novel tetrapeptide. *J. Pept. Res.* **2002**, *59*, 249−256.
(59) Ananthananarayanan, V. S.; Cameron, T. S. Proline-containing β-turns. *Int. J. Pept. Protein Res.* **1998**, *31*, 399−411.
(60) Lapić, J.; Siebler, D.; Heinze, K.; Rapić, V. Conformational analysis of heteroannularly substituted ferrocene oligoamides. *Eur. J. Inorg. Chem.* **2007**, *2007*, 2014−2024.
(61) Kaplan, S.; Colak, M.; Hosgoren, H.; Pirinccioglu, N. Design of L-Lysine-Based Organogelators and Their Applications in Drug Release Processes. *ACS Omega.* **2019**, *4*, 12342−12356.
(62) Berger, N.; Wollny, LJ. B.; Sokkar, P.; Mittal, S.; Mieres-Perez, J.; Stoll, R.; Sander, W.; Sanchez-Garcia, E. Solvent-Enhanced Conformational Flexibility of Cyclic Tetrapeptides. *Chemphyschem.* **2019**, *20*, 1664−1670.
(63) Vincenzi, M.; Mercurio, F. A.; Leone, M. NMR Spectroscopy in the Conformational Analysis of Peptides: An Overview. *Curr. Med. Chem.* **2021**, *28*, 2729−2782.
(64) Nerli, S.; McShan, A. C.; Sgourakis, N. G. Chemical shift-based methods in NMR structure determination. *Prog. Nucl. Magn. Reson. Spectrosc.* **2018**, *106*−*107*, 1−25.
(65) Pardi, A.; Wagner, G.; Wuthrich, K. Protein conformation and proton nuclear-magnetic-resonance chemical shifts. *Eur. J. Biochem.* **1983**, *137*, 445−454.
(66) Gellman, S. H.; Dado, G. P.; Liang, G.-B.; Adams, B. R. Conformation-directing effects of a single intramolecular amide-amide hydrogen bond: variable-temperature NMR and IR studies on a homologous diamide series. *J. Am. Chem. Soc.* **1991**, *113*, 1164−1173.
(67) Wagner, G.; Pardi, A.; Wuethrich, K. Hydrogen bond length and proton NMR chemical shifts in proteins. *J. Am. Chem. Soc.* **1983**, *105*, 5948−5949.
(68) Raghothama, S. R.; Awasthi, S. K.; Balaram, P. β-Hairpin nucleation by Pro-Gly β-turns. Comparison of D-Pro-Gly and L-Pro-Gly sequences in an apolar octapeptide. *J. Chem. Soc., Perkin Trans.* **1998**, *2*, 137−144.
(69) Liu, J.-Y.; Sun, X.-Y.; Tang, Q.; Song, J.-J.; Li, X.-Q.; Gong, B.; Liu, R.; Lu, Z.-L. An unnatural tripeptide structure containing intramolecular double H-bond mimics a turn-hairpin conformation. *Org. Biomol. Chem.* **2021**, *19*, 4359−4363.
(70) Llinás, M.; Klein, M. P. Solution conformation of the ferrichromes. VI. Charge relay at the peptide bond. Proton magnetic resonance study of solvation effects on the amide electron density distribution. *J. Am. Chem. Soc.* **1975**, *97*, 4731−4737.
(71) Stevens, E. S.; Sugawara, N.; Bonora, G. M.; Toniolo, C. Conformational analysis of linear peptides. 3. Temperature dependence of NH chemical shifts in chloroform. *J. Am. Chem. Soc.* **1980**, *102*, 7048−7050.
(72) Kessler, H. Conformation and Biological Activity of cyclic Peptides. *Angew. Chem., Int. Ed. Engl.* **1982**, *21*, 512−523.
(73) Iqbal, M.; Balaram, P. Aggregation of apolar peptides in organic solvents. Concentration dependence of 1H-nmr parameters for peptide NH groups in 310 helical decapeptide fragment of suzukacillin. *Biopolymers* **1982**, *21*, 1427−1433.
(74) Kumar, E. K. S. V.; Balaram, P. Stereochemistry of a-aminoisobutyric acid peptides in solution. Helical conformations of protected decapeptides with repeating Aib-L-Ala and Aib-L-Val sequences. *Biopolymers* **1983**, *22*, 2133−2140.
(75) Andersen, N. H.; Neidigh, J. W.; Harris, S. M.; Lee, G. M.; Liu, Z.; Tong, H. Extracting Information from the Temperature Gradients of Polypeptide NH Chemical Shifts. 1. The Importance of Conformational Averaging. *J. Am. Chem. Soc.* **1997**, *119*, 8547−8561.

https://doi.org/10.1021/acs.organomet.4c00248
Organometallics 2024, 43, 2608−2625

(76) Baxter, N. J.; Williamson, M. P. Temperature dependence of 1H chemical shifts in proteins. *J. Biomol. NMR* **1997**, *9*, 359−369.
(77) Cierpicki, T.; Otlewski, J. Amide proton temperature coefficients as hydrogen bond indicators in proteins. *J. Biomol. NMR* **2001**, *21*, 249−261.
(78) Cierpicki, T.; Zhukov, I.; Byrd, R. A.; Otlewski, J. Hydrogen bonds in human ubiquitin reflected in temperature coefficients of amide protons. *J. Magn. Reson.* **2002**, *157*, 178−180.
(79) Sarkar, S. K.; Young, P. E.; Sullivan, C. E.; Torchia, D. A. Detection of cis and trans X-Pro peptide bonds in proteins by 13C NMR: application to collagen. *Proc. Natl. Acad. Sci. U S A* **1984**, *81*, 4800−4803.
(80) O'Neal, K. D.; Chari, M. V.; Mcdonald, C. H.; Cook, R. G.; Yu-Lee, L. Y.; Morrisett, J. D.; Shearer, W. T. Multiple cis-trans conformers of the prolactin receptor proline-rich motif (PRM) peptide detected by reverse-phase HPLC, CD and NMR spectroscopy. *Biochem. J.* **1996**, *315*, 833−844.
(81) Chatterjee, B.; Saha, I.; Raghothama, S.; Aravinda, S.; Rai, R.; Shamala, N.; Balaram, P. Designed Peptides with Homochiral and Heterochiral Diproline Templates as Conformational Constraints. *Chem.—Eur. J.* **2008**, *14*, 6192−6204.
(82) Ishimoto, B.; Tonan, K.; Ikawa, S. Coupling of intramolecular hydrogen bonding to the cis-to-trans isomerization of a proline imide bond of small model peptides. *Spectrochim. Acta A Mol. Biomol. Spectrosc.* **2000**, *56*, 201−209.
(83) Deetz, M. J.; Fahey, J. E.; Smith, B. D. NMR studies of hydrogen bonding interactions with secondary amide and urea groups. *J. Phys. Org. Chem.* **2001**, *14*, 463−467.
(84) Pignataro, M. F.; Herrera, M. G.; Dodero, V. I. Evaluation of Peptide/Protein Self-Assembly and Aggregation by Spectroscopic Methods. *Molecules.* **2020**, *25*, 4854−4888.
(85) Rogers, D. M.; Jasim, S. B.; Dyer, N. T.; Auvray, F.; Réfrégiers, M.; Hirst, J. D. *Chem.* **2019**, *5*, 2751−2774.
(86) Moriuchi, T. Helical Chirality of Ferrocene Moieties in Cyclic Ferrocene-Peptide Conjugates. *Chem.—Eur. J.* **2022**, *2022*, No. e202100902.
(87) Snegur, L. V. Ferrocene and Its Derivatives: Celebrating the 70th Anniversary of Its Discovery. *Inorganics* **2022**, *10*, 226−246.
(88) Rodionov, A. N.; Snegur, L. V.; Belousov, Yu. A.; Korlyukov, A. A.; Simenel, A. A. The nature of ferrocenylalkylating agent in the acid-catalyzed reactions with ferrocenyl(phenyl)methanol. *Russ. Chem. Bull.* **2021**, *70*, 1900−1907.
(89) Shlar, I.; Droby, S.; Choudhary, R.; Rodov, V. The mode of antimicrobial action of curcumin depends on the delivery system: monolithic nanoparticles *vs.* supramolecular inclusion complex. *RSC Adv.* **2017**, *7*, 42559−42569.
(90) Mishra, A. K.; Choi, J.; Moon, E.; Baek, K.-H. Tryptophan-Rich and Proline-Rich Antimicrobial Peptides. *Molecules* **2018**, *23*, 815−838.
(91) Saint Jean, K. D.; Henderson, K. D.; Chrom, C. L.; Abiuso, L. E.; Renn, L. M.; Caputo, G. A. Effects of Hydrophobic Amino Acid Substitutions on Antimicrobial Peptide Behavior. *Probiotics Antimicrob. Proteins.* **2018**, *10*, 408−419.
(92) Schifano, N. P.; Caputo, G. A. Investigation of the Role of Hydrophobic Amino Acids on the Structure−Activity Relationship in the Antimicrobial Venom Peptide Ponericin L1. *J. Membr. Biol.* **2022**, *255*, 537−551.
(93) Zhang, J.; Fu, Y.; Yang, P.; Liu, X.; Li, Y.; Gu, Z. ROS Scavenging Biopolymers for Anti-Inflammatory Diseases: Classification and Formulation. *Adv. Mater. Interfaces* **2020**, *7*, No. 2000632.
(94) Ternansky, R. J.; Draheim, S. E.; Pike, A. J.; Counter, F. T.; Eudaly, J. A.; Kasher, J. S. Structure-activity relationship within a series of pyrazolidinone antibacterial agents. 2. Effect of side-chain modification on in vitro activity and pharmacokinetic parameters. *J. Med. Chem.* **1993**, *36*, 3224−3229.
(95) Bugarinović, J. P.; Pešić, M. S.; Minić, A.; Katanić, J.; Ilić-Komatina, D.; Pejović, A.; Mihailović, V.; Stevanović, D.; Nastasijević, B.; Damljanović, I. Ferrocene-containing tetrahydropyrazolopyrazolones: Antioxidant and antimicrobial activity. *J. Inorg. Biochem.* **2018**, *189*, 134−142.
(96) López-Alarcón, C.; Lissi, E. A novel and simple ORAC methodology based on the interaction of Pyrogallol Red with peroxyl radicals. *Free Radic. Res.* **2006**, *40*, 979−85.
(97) Pellegrini, N.; Serafini, M.; Colombi, B.; Del Rio, D.; Salvatore, S.; Bianchi, M.; Brighenti, F. Total antioxidant capacity of plant foods, beverages and oils consumed in Italy assessed by three different in vitro assays. *J. Nutr.* **2003**, *133*, 2812−2819.
(98) Perea-Domínguez, X. P.; Hernández-Gastelum, L. Z.; Olivas-Olguin, H. R.; Espinosa-Alonso, L. G.; Valdez-Morales, M.; Medina-Godoy, S. Phenolic composition of tomato varieties and an industrial tomato by-product: free, conjugated and bound phenolics and antioxidant activity. *J. Food Sci. Technol.* **2018**, *55*, 3453−3461.
(99) Schröder, M.; Petrova, M.; Vlahova, Z.; Dobrikov, G. M.; Slavchev, I.; Pasheva, E.; Ugrinova, I. In Vitro Anticancer Activity of Two Ferrocene-Containing Camphor Sulfonamides as Promising Agents against Lung Cancer Cells. *Biomedicines.* **2022**, *10*, 1353−1370.
(100) Koszytkowska-Stawińska, M.; Buchowicz, W. Ferrocene-triazole conjugates: do we know why they are biologically active? *Dalton Trans.* **2023**, *52*, 1501−1517.
(101) Zeng, L.; Tang, M.; Pi, C.; Zheng, J.; Gao, S.; Chabanne, T.; Chauvin, R.; Cheng, W.; Lin, H.; Xu, R.; Cui, X. Novel Ferrocene Derivatives Induce Apoptosis through Mitochondria-Dependent and Cell Cycle Arrest via PI3K/Akt/mTOR Signaling Pathway in T Cell Acute Lymphoblastic Leukemia. *Cancers (Basel)* **2021**, *13*, 4677−4691.
(102) Li, L.; Thomas, R. M.; Suzuki, H.; de Brabander, J. K.; Wang, X.; Harran, P. G. A small molecule Smac mimic potentiates TRAIL- and TNFalpha-mediated cell death. *Science* **2004**, *305*, 1471−1474.
(103) Mabonga, L.; Kappo, A. P. Peptidomimetics: A Synthetic Tool for Inhibiting Protein−Protein Interactions in Cancer. *Int. J. Pept. Res. Ther.* **2020**, *26*, 225−241.
(104) Boyd, M. R.; Paull, K. D. Some practical considerations and applications of the national cancer institute in vitro anticancer drug discovery screen. *Drug. Develop. Res.* **1995**, *34*, 91−109.
(105) *Schrödinger Release 2019−4: MacroModel*; Schrödinger, LLC: New York, 2019.
(106) Mohamadi, F.; Richards, N. G. J.; Guida, W. C.; Liskamp, R.; Lipton, M.; Caufield, C.; Chang, G.; Hendrickson, T.; Still, W. C. Macromodel—An integrated software system for modeling organic and bioorganic molecules using molecular mechanics. *J. Comput. Chem.* **1990**, *11*, 440−467.
(107) Frisch, M. J.; Trucks, G. W.; Schlegel, H. B.; Scuseria, G. E.; Robb, M. A.; Cheeseman, J. R.; Scalmani, G.; Barone, V.; Petersson, G. A.; Nakatsuji, H.; Li, X.; Caricato, M.; Marenich, A. V.; Bloino, J.; Janesko, B. G.; Gomperts, R.; Mennucci, B.; Hratchian, H. P.; Ortiz, J. V.; Izmaylov, A. F.; Sonnenberg, J. L.; Williams-Young, D.; Ding, F.; Lipparini, F.; Egidi, F.; Goings, J.; Peng, B.; Petrone, A.; Henderson, T.; Ranasinghe, D.; Zakrzewski, V. G.; Gao, J.; Rega, N.; Zheng, G.; Liang, W.; Hada, M.; Ehara, M.; Toyota, K.; Fukuda, R.; Hasegawa, J.; Ishida, M.; Nakajima, T.; Honda, Y.; Kitao, O.; Nakai, H.; Vreven, T.; Throssell, K.; Montgomery, J. A.; Peralta, J. E.; Ogliaro, F.; Bearpark, M. J.; Heyd, J. J.; Brothers, E. N.; Kudin, K. N.; Staroverov, V. N.; Keith, T. A.; Kobayashi, R.; Normand, J.; Raghavachari, K.; Rendell, A. P.; Burant, J. C.; Iyengar, S. S.; Tomasi, J.; Cossi, M.; Millam, J. M.; Klene, M.; Adamo, C.; Cammi, R.; Ochterski, J. W.; Martin, R. L.; Morokuma, K.; Farkas, O.; Foresman, J. B.; Fox, D. J. *Gaussian 16*, Revision C.01, Gaussian, Inc.: Wallingford CT, 2016.
(108) Mennucci, B.; Cancès, E.; Tomasi, J. Evaluation of Solvent Effects in Isotropic and Anisotropic Dielectrics and in Ionic Solutions with a Unified Integral Equation Method: Theoretical Bases, Computational Implementation, and Numerical Applications. *J. Phys. Chem. B* **1997**, *101*, 10506−10517.
(109) Keith, T. A., *AIMAll*, Version 19.02.13; TK Gristmill Software: Overland Park, KS, USA, 2017.

https://doi.org/10.1021/acs.organomet.4c00248
Organometallics 2024, 43, 2608−2625

(110) Koch, U.; Popelier, P. L. A. Characterization of C-H-O Hydrogen Bonds on the Basis of the Charge Density. *J. Phys. Chem.* **1995**, *99*, 9747−9754.
(111) Rigaku Oxford Diffraction. *CrysAlisPro Software System*, Version 1.171.39.46; Rigaku Corporation: Oxford, U.K., 2018.
(112) Sheldrick, G. M. SHELXT-integrated space-group and crystal-structure determination. *Acta Crystallogr. A Found. Adv.* **2015**, *71*, 3−8.
(113) Sheldrick, G. M. Crystal structure refinement with SHELXL. *Acta Crystallogr. C* **2015**, *C71*, 3−8.
(114) Spek, A. L. CheckCIF validation ALERTS: What they mean and how to respond. *Acta Crystallogr. E76* **2020**, *76*, 1−11.
(115) Farrugia, L. J. ORTEP-3 for Windows-a version of ORTEP-III with a Graphical User Interface (GUI). *J. Appl. Crystallogr.* **1997**, *30*, 565.
(116) Macrae, C. F.; Sovago, I.; Cottrell, S. J.; Galek, P. T. A.; McCabe, E. P.; Platings, M.; Shields, G. P.; Stevens, J. S.; Towler, M.; Wood, P. A. Mercury 4.0: From visualization to analysis, design and prediction. *J. Appl. Crystallogr.* **2020**, *53*, 226−235.
(117) Brand-Williams, W.; Cuvelier, M. E.; Berset, C. Use of a freeradical method to evaluate antioxidant activity. *Food Sci. Technol.* **1995**, *28*, 25−30.
(118) Re, R.; Pellegrini, N.; Proteggente, A.; Pannala, A.; Yang, M.; Rice-Evans, C. Antioxidant activity applying an improved ABTS radical cation decolorization assay. *Free Radic. Biol. Med.* **1999**, *26*, 1231−1237.

https://doi.org/10.1021/acs.organomet.4c00248
Organometallics 2024, 43, 2608−2625